Karlsruher Institut für Technologie

Separate-effects tests on the investigation of high-temperature oxidation behavior and mechanical properties of Zircaloy-2 to be used in the SFP PWR tests

Report prepared in the framework of the
OECD/NEA SFP Project

M. Steinbrück, M. Jung, M. Walter
Institute for Materials Research

Karlsruhe 2010

KIT – University of the State of Baden-Wuerttemberg and National Laboratory of the Helmholtz Association

Abstract

The thermo-hydraulic and ignition behavior of full-scale Pressurized Water Reactor (PWR) fuel assembly mock-ups during hypothetic spent fuel pool Loss of Coolant Accidents (LOCA) will be investigated in the frame of the OECD-NEA Sandia Fuel Program (SFP).

The choice of the cladding alloy has been intensively discussed in the initial phase of the project. The PWR cladding alloys Zircaloy-4 or ZIRLO have been originally foreseen to be used in these tests. Due to problems regarding availability and proprietary rights of these materials, finally the Boiling Water Reactor (BWR) material Zircaloy-2 was selected as heater rod material. The main arguments for Zry-2 were availability of material and all data, the positive experience with the material during the BWR test series and the very similar properties of Zry-2 and Zry-4. Some participants asked for a proof of the latter statement, especially because the database on Zry-2 is scarce in comparison with Zry-4. In this context KIT performed a series of separate-effects tests (SETs) to confirm the similarity of the two alloys and to deliver corresponding data. The following report presents the results of isothermal and transient oxidation tests of Zry-2 and Zry-4 in air atmosphere, including simulations of the planned pre-ignition and ignition tests, as well as results of mechanical tests.

Isothermal and transient experiments were conducted in a commercial thermal balance coupled with a mass spectrometer up to temperatures of 1600 °C. Ring compression and tensile tests were performed with a universal testing machine from Instron.

The results of the extensive experimental program revealed very similar oxidation behaviour of the two alloys Zircaloy-2 and Zircaloy-4 in the temperature range investigated. So, there are no concerns regarding the use of the BWR alloy Zircaloy-2 in the PWR SFP test series at Sandia National Laboratories from this point of view. During the planned pre-ignition tests only very low pre-oxidation of the cladding and so insignificant effect on the main ignition test is expected. The point in time of the ignition of the bundle strongly influences the starting conditions for the further progression of the test, especially the degree of pre-oxidation and therewith the amount of remaining metal.

The mechanical properties of the two alloys in the as-received state and the heater cladding are significantly different. The manufacturing process of the heater rods caused increase of strength and reduction of ductility. Further strong changes of mechanical properties are expected during course of the tests due to oxidation. This has to be taken into account for the analyses of the tests.

TABLE OF CONTENTS

LIST OF TABLES

LIST OF FIGURES

1 Introduction

In the frame of the OECD-NEA Sandia Fuel Program (SFP), the thermo-hydraulic and ignition behavior of full-scale Pressurized Water Reactor (PWR) fuel assembly mock-ups during hypothetic spent fuel pool Loss of Coolant Accidents (LOCA) will be investigated.

The choice of the cladding alloy has been intensively discussed in the initial phase of the project. The PWR cladding alloys Zircaloy-4 or ZIRLO have been originally foreseen to be used in these tests. Due to problems regarding availability and proprietary rights of these materials, finally the Boiling Water Reactor (BWR) material Zircaloy-2 was selected as heater rod material. The main arguments for Zry-2 were availability of material and all data, the positive experience with the material during the BWR test series and the very similar properties of Zry-2 and Zry-4. Some participants asked for a proof of the latter statement. The database on Zry-2 is scarce in comparison with Zry-4 because severe accident research in the past was more concentrated on PWR.

In this context KIT performed a series of separate-effects tests (SETs) to confirm the similarity of the two alloys and to deliver corresponding data. The following report presents the results of isothermal and transient oxidation tests of Zry-2 and Zry-4 in air atmosphere, including simulations of planned pre-ignition and ignition tests, as well as results of mechanical tests.

2 Experimental Details

2.1 Thermal balance test set-up

All oxidation experiments were performed in a commercial thermal balance (NETZSCH STA-409) coupled via a capillary with a 6-mm quadrupole mass spectrometer (NETZSCH Aeolos). Figure 2-1 gives a schematic of the set-up. The gases (in these tests only Ar and air) are supplied via Bronkhorst flow controllers at the lower part of the vertical tube furnace. Argon flows through the balance containment into the furnace; the reaction gas air is directly injected into the reaction tube to prevent contamination of the balance and to ensure a well-defined gas mixture in the furnace. All gases used were highly pure gases with less than 1 or 10 ppm impurities.

The specimens were supported by an yttria plate to prevent interactions between the Zircaloy and the alumina sample plate. The temperature of the furnace was controlled by the thermocouple located directly below the sample plate (STC = sample temperature control).

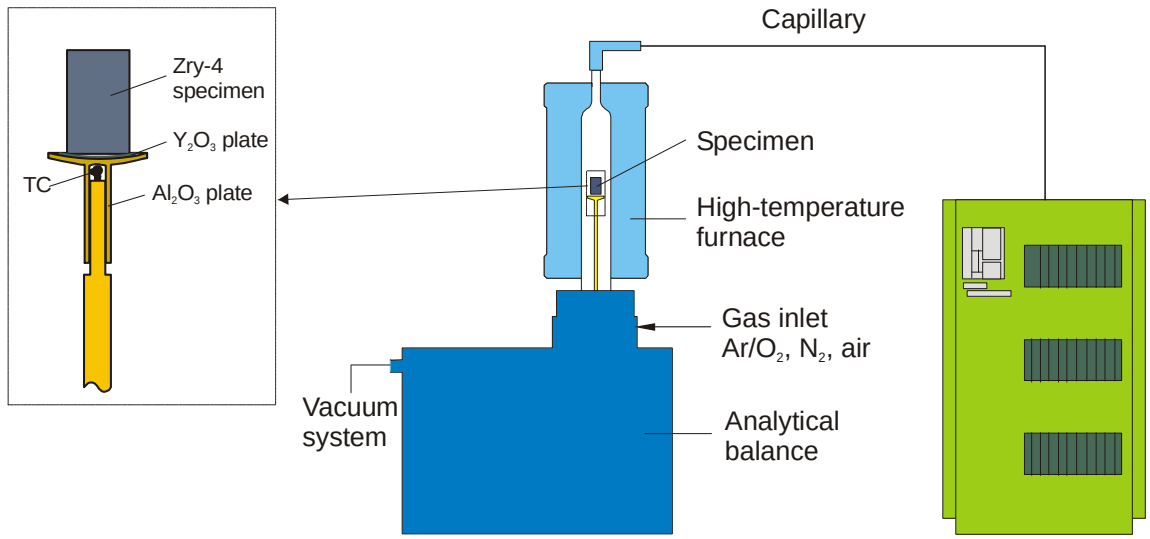

Fig. 2-1 Schematic view of the thermal balance coupled with MS and TG measuring head with specimen.

2.2 Specimens

4x1 m Zry-2 tube segments as well as two 1-m prototype heater segments were delivered by SNL via USNRC for these investigations. Zircaloy-4 cladding rods were available at KIT. The composition of both alloys is very similar with approx. 1.5 wt-% tin as major alloying element. A detailed table with the composition data, taken from an ATI Wah Chang Technical Data Sheet [8], can be found in Appendix A.

The tubes were cut into 2-cm segments, deburred and ground at the cutting edges, and cleaned in an ultrasonic bath with acetone. Figure 2-2 shows the tubes as received and a 2-cm sample prepared for oxidation test. The heater rods still contained MgO packing and Nichrome heater elements which had to be removed before the oxidation tests.

Fig. 2-2 Zircaloy-2 rod (top) and two prototype heaters as received (left) and sample for TG test (right)

The Zry-2 tubing is fabricated with an about 100 µm thick pure zirconium liner on the inside surface (Fig 2-3). This does not influence the bundle tests, but the TG tests with oxidation of the inner and outer surfaces. So, it was decided to remove the inner Zr liner by a reaming technique. The Zry-4 tube segments were also reamed to adapt the cladding wall thicknesses and make the two kinds of specimens more comparable. The dimensions of all specimens investigated are summarized in Table 2-1.

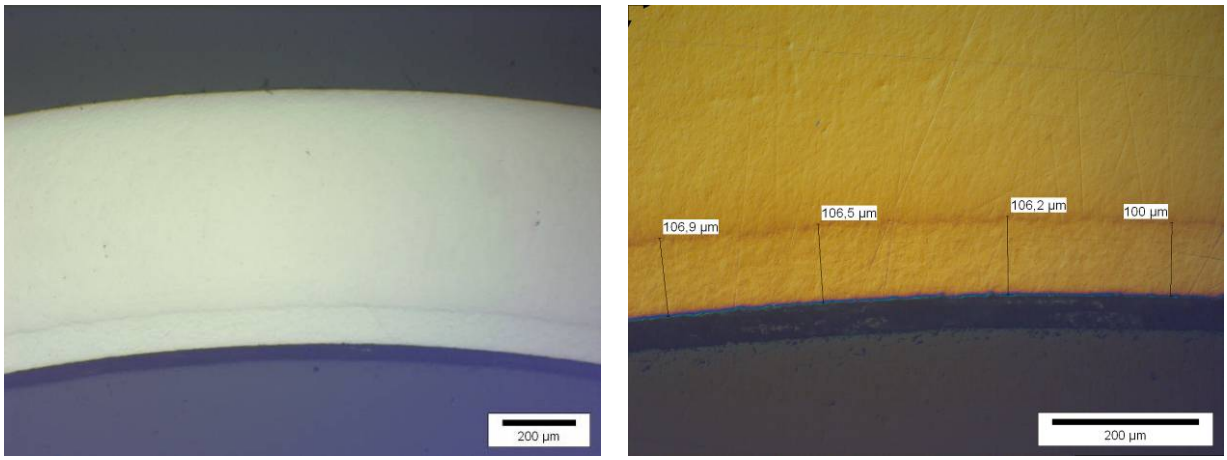

Fig. 2-3 Micro images of the Zry-2 cladding with inner zirconium liner. Left: Bright field image, right: interference contrast image with measurements

Tab. 2-1 Sample dimensions

	Zry-4 as-received	Zry-4 reamed	Zry-2 as-received	Zry-2 reamed	Zry-2 heater prototype
Outer diameter (mm)	10,735	10,732	11,14	11,131	9,55
Inner diameter (mm)	9,37	9,83	9,82	10,22	8,054
Wall thickness (mm)	0,683	**0,451**	0,66	**0,456**	0,748
Inner removal (mm)	0,232		0,205		

For mechanical test, 20 cm rod segments were prepared from the as-received tubing for tensile tests and 1 cm samples for ring pressure tests.

2.3 Oxidation test program

Isothermal tests with Zry-2 and Zry-4 as reference were conducted with as-received and reamed specimens in the temperature range 600-1400 °C with 100 K steps for determination of oxidation kinetics. More prototypic transient experiments were performed at three heating rates (5, 20, 50 K/min) only with machined samples. Some selected tests were done with

heater rods. The test conditions are summarized in Tables 2-2 and 2-3. Additionally, the pre-ignition tests as well as the ignition test till start of temperature runaway were simulated according to the results of pre-test calculations with MELCOR.

Tab. 2-2 Test program isothermal oxidation

Temperature	Zry-2 as-received	Zry-4 as-received	Zry-2 reamed	Zry-4 reamed	Zry-2 heater
600°C	60h	60h	60h	60h	
700°C	17h	17h	17h	17h	
800°C	7h	7h	7h	7h	
900°C	2h30min	2h30min	1h20min	1h20min	2h30min
1000°C	1h20min, 30min	1h20min, 30min	45min	45min	30min
1100°C	20min	20min	15min	15min	20min
1200°C	15min	15min	15min	15min	
1300°C	10min	10min	7,5min	7.5min	
1400°C	10min	10min	7min	7min	

Tab. 2-3 Test program transient oxidation

Heating rate	Zry-2 reamed	Zry-4 reamed
5 K/min	274min	274min
20 K/min	65min	65min
50 K/min	25min	25min

2.4 Test conduct

For isothermal tests, the specimens were heated with a rate of 30 K/min in argon to the test temperature and 10 min thermally equilibrated. Then, the oxidising gas (air) was injected till maximum approx. 25 wt% mass gain was obtained or for a pre-defined time. The tests were finished by switching off the oxidising gas and cooling the furnace as fast as possible in argon atmosphere.

Complete oxidation of Zircaloy leads to a mass gain of 35 wt%. The target of less than 25 wt% mass gain was chosen in order to have enough remaining metal phase for metallographic examinations. In the transient tests, air was injected from the beginning of the test till the end of the heating phase.

The argon flow rate during all the tests was 3 l/h. Argon was used to protect the balance and as reference gas for the mass spectrometer measurements. The typical flow rate for air was 10 l/h. At 1300 and 1400 °C some tests were conducted with 30 l/h air to prevent oxygen starvation conditions.

Figure 2-4 shows typical test conducts of isothermal and transient tests. The main parameters of all tests conducted in the thermal balance are summarised in Appendix B.

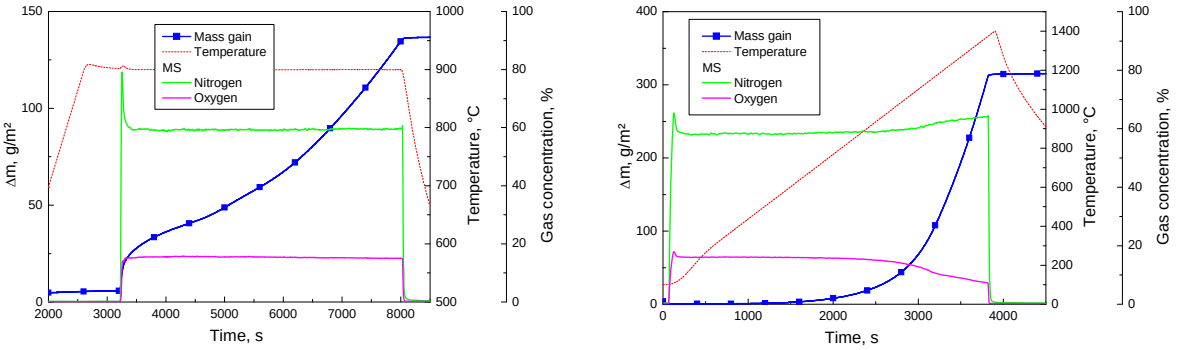

Fig. 2-4 Typical examples of test conduct of isothermal (left) and transient (right) oxidation experiments in air showing temperature, mass gain and gas composition measured by mass spectrometer (MS) in the off-gas

2.5 Post-test examinations

Macro photos were taken of all specimens after the tests. Then the specimens were embedded in epoxy resin, cut, ground and polished for metallographic examinations by optical microscopy. Light-microscopic examinations were performed with bright-field illumination, polarized light and interference contrast.

As already mentioned the specimens were open and thus allowed inner and outer oxidation. Because the experimental conditions e.g. regarding gas flow are better defined for the external surface of the tube segments it is recommended to focus attention on examination of external oxide scales.

2.6 Mechanical tests

Mechanical tests were carried out with a universal testing machine from Instron (model 4505), equipped with a 50 kN load cell. For ring compression tests, an experimental set-up was used as shown in Fig. 2-5. To measure the exact displacement during a test, the rings were compressed between two SiC-disks (very high stiffness) within the machine which are connected via Al_2O_3-plates with a high resolution LVDT (linear variable differential transformer) position sensor.

To perform tensile tests on cladding sections with a length of ca. 200 mm, a set-up was used as shown in Fig. 2-6. Here, the tubes, equipped with exact fitting end plugs, are clamped in special grip holders for round bars. The heater rods were tested including the heater wire

and MgO filler. The deformation of a specimen during a test was measured by using a CCD-camera system allowing the determination of the global and local strains with high resolutions.

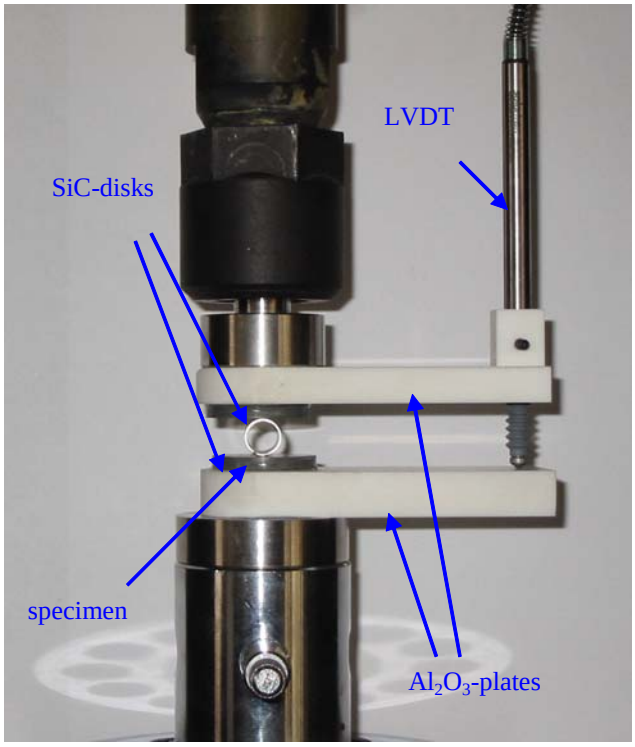

Fig. 2-5 Test set-up for ring compression tests

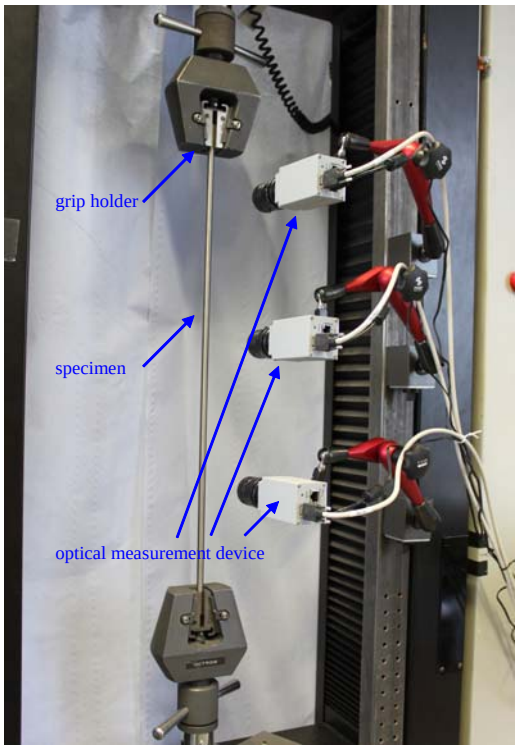

Fig. 2-6 Test set-up for tensile tests

3 Results

3.1 Isothermal oxidation tests with as-received and heater cladding

First tests were conducted with as-received cladding tube segments and heater tubes in order to get a feeling for the material and to investigate the influence of the inner Zr liner and the heater manufacturing process on the oxidation behavior of the alloy. Figure 3-1 presents the thermo-gravimetric curves of all tests in the temperature range 600-1400 °C. Especially at lower temperatures up to 1000 °C the beneficial effect of the inner Zr liner is obvious. After a certain time (indicated in Fig. 3-1) of very similar oxidation kinetics the oxidation rates of Zry-4 strongly increase in comparison to the Zry-2. The main reason for this behavior is the higher susceptibility of the Zr-Sn alloys for breakaway oxidation in comparison to pure zirconium. Due to phase changes in the oxide phase stresses are build up in the oxide scale which finally lead to the formation of cracks and the loss or reduction of the protective effect of the oxide scale.

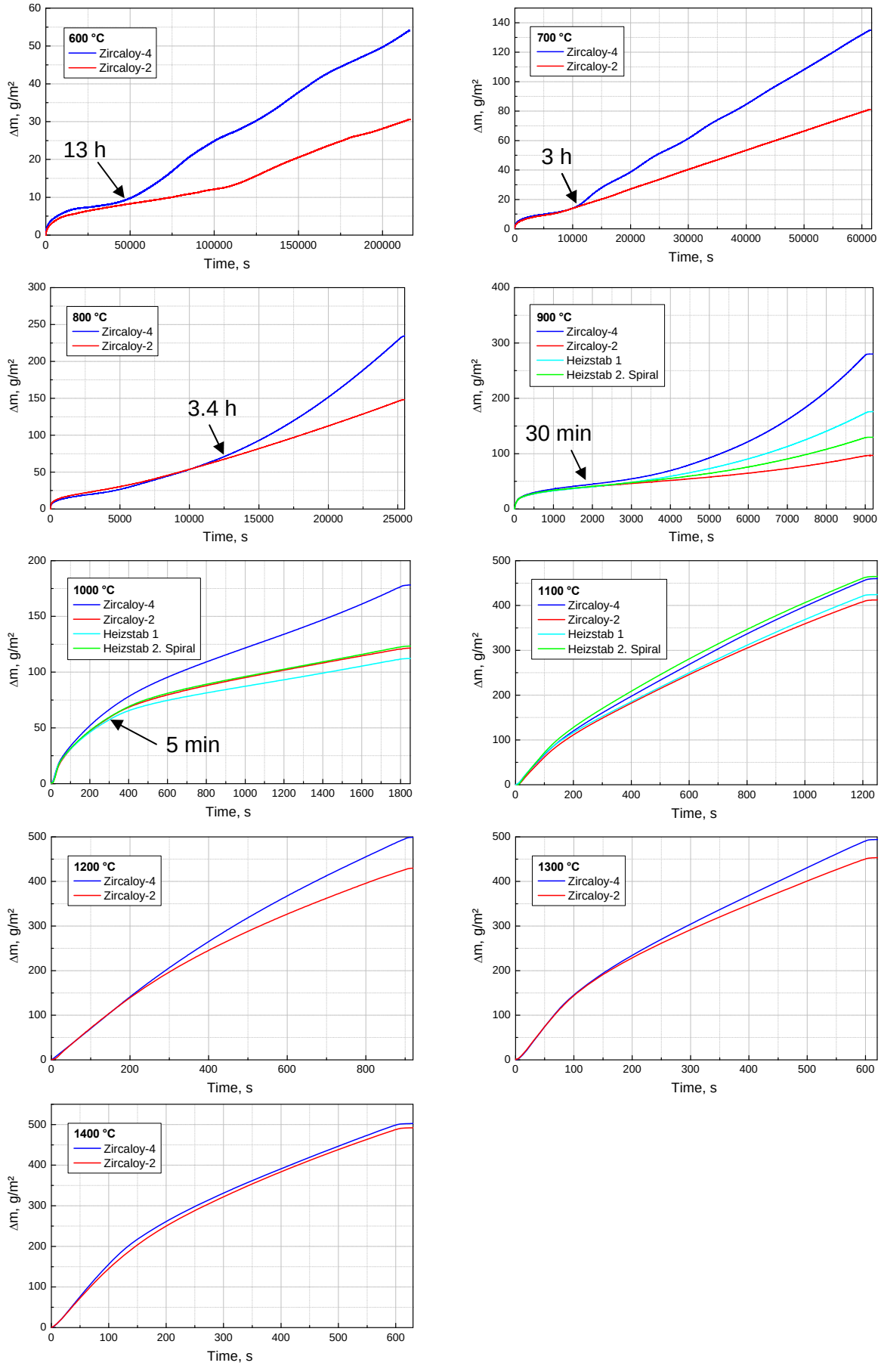

Fig. 3-1 Mass gain during isothermal oxidation of as-received Zry-2 and Zry-4 in air in the temperature range 600-1400 °C *(Heizstab=Heater rod)*

The oxidation rates are additionally increased due to the formation of nitrides at the phase boundary metal-oxide and their re-oxidation which are also connected with strong changes in the specific volume. The mechanism of air oxidation is described in more detail in [1] and [2].

Figures 3-2 and 3-3 give examples of post-test appearance and metallographic examinations which show very similar external oxide scales with nitride formation and the protective effect of the Zr liner for the inner oxidation of the Zry-2 samples. Macro and micro images of all specimens are presented in Annexes C and D. They generally show a very similar behavior of the two alloys and partially axially changing surfaces and diameters. The positive effect of the inner Zr liner for Zry-2 is confirmed at all temperatures.
Very strong nitride formation connected with very porous oxide/nitride scales is seen in the temperature range 1000-1300 °C. Starting at 1400 °C the effect of nitrogen attack decreases as was already seen in former studies, possibly caused by raising ductility of the oxide with temperature.

Zry-4 Zry-2 Heater 1 Heater 2

Fig. 3-2 Post-test appearance of as-received specimens after 30 min isothermal oxidation in air at 1000 °C

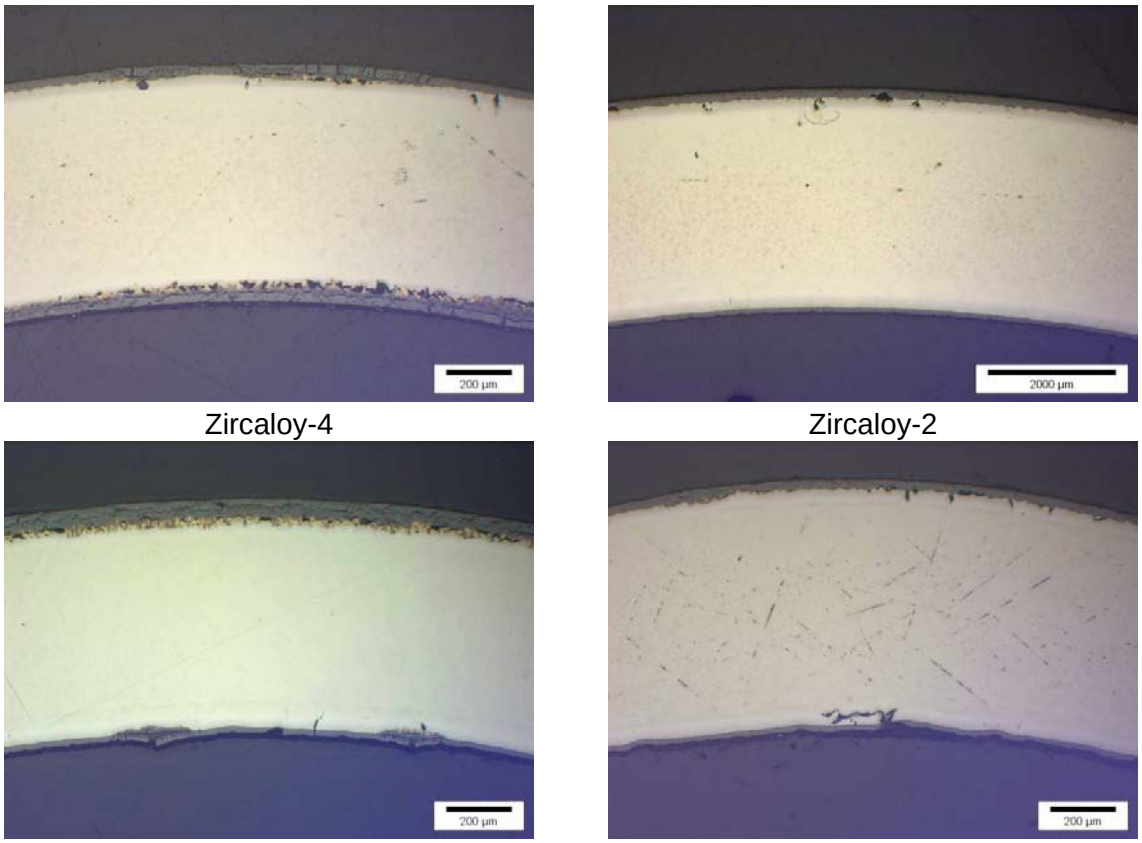

Fig. 3-3 Micrographs of as-received specimens after oxidation in air at 900 °C

3.2 Isothermal oxidation tests with machined specimens

The second and main test series was conducted with machined specimens, i.e. with specimens without inner Zr liner for Zry-2 as well as with very comparable wall thicknesses and surface qualities of both alloys.

Figure 3-4 gives an overview of all TG measurements at 600-1400 °C. The curves obtained for the two alloys are almost identical over the whole temperature range investigated. Only at 700 °C and 900 °C a moderate deviation between the two signals was measured after about 7000 and 1700 s, respectively. Again, a transformation from parabolic/cubic oxidation kinetics (determined by the growing protective oxide scales) to linear or even accelerating ones is observed at temperatures below 1100 °C. The wavelike appearance of the curves at 600 and 700 °C after transition is an indication of recurring processes of oxide scale growth and degradation due to crack formation and/or shattering. The almost linear appearance of the TG curve at 1300 °C and the standard air flow rate of 10 l/h is due to oxygen starvation caused by the very high oxidation rates at this temperature. This was also confirmed by mass spectrometer measurements. Therefore, the air flow rate was increased to 29 l/h (max. controller capacity) at temperatures of 1300 and 1400 °C.

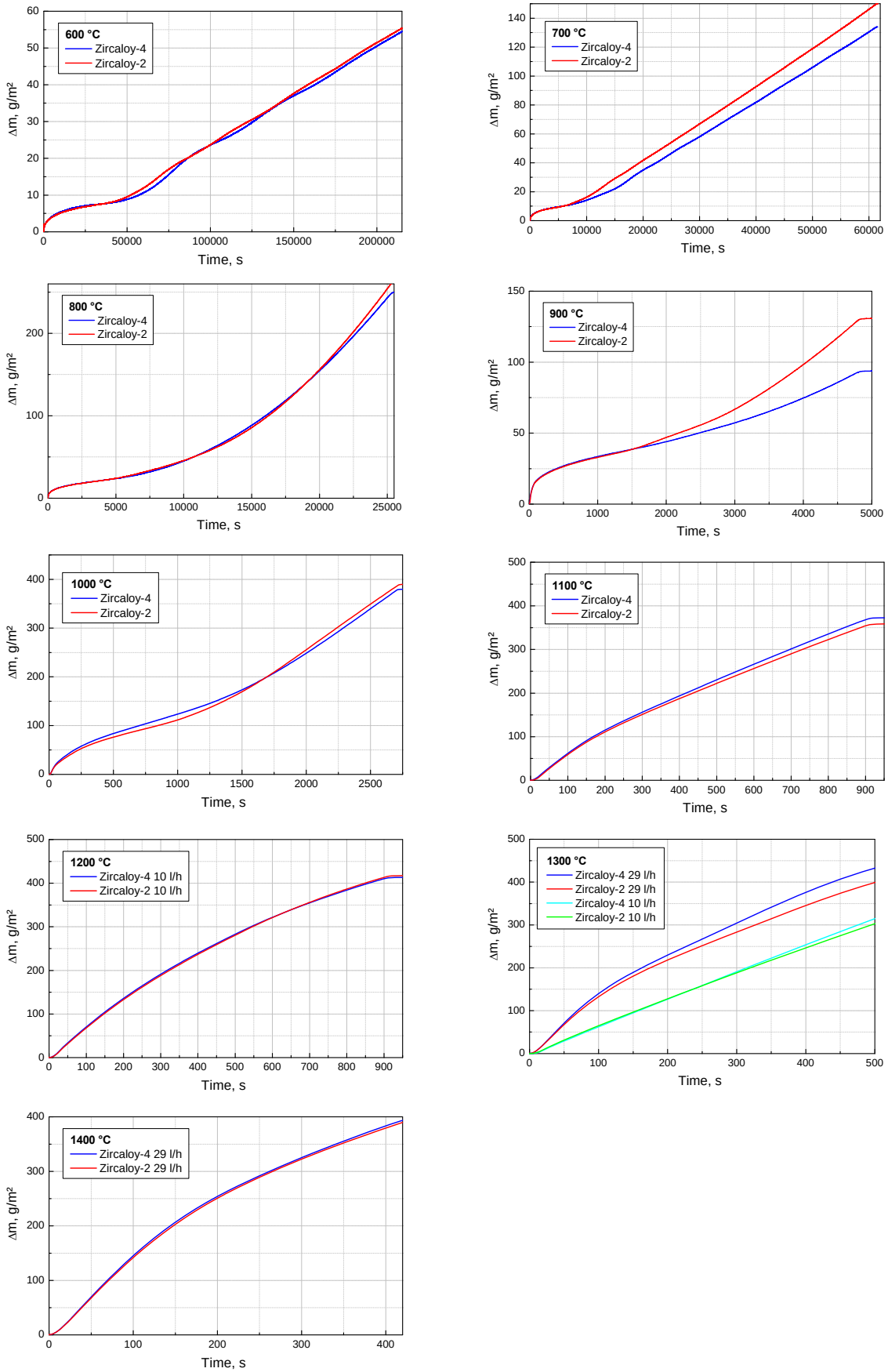

Fig. 3-4 Mass gain during isothermal oxidation of machined Zry-2 and Zry-4 in air in the temperature range 600-1400 °C

Obviously, the reaming process somehow influenced the samples as can be seen in Fig. 3-5. The oxidation is a bit faster for Zry-4 specimens after reaming in comparison to the as-received ones.

As already mentioned in section 3.1, all post-test images are compiled in Annexes C and D and here only illustrative examples are shown in Figs. 3-6 and 3-7. There is no difference in the post-test appearance and microstructure visible for the two alloys. The micrographs impressively reveal the accelerating formation of zirconium nitride at the metal-oxide boundary below a more or less dense oxide scale formed initially (before the transition).

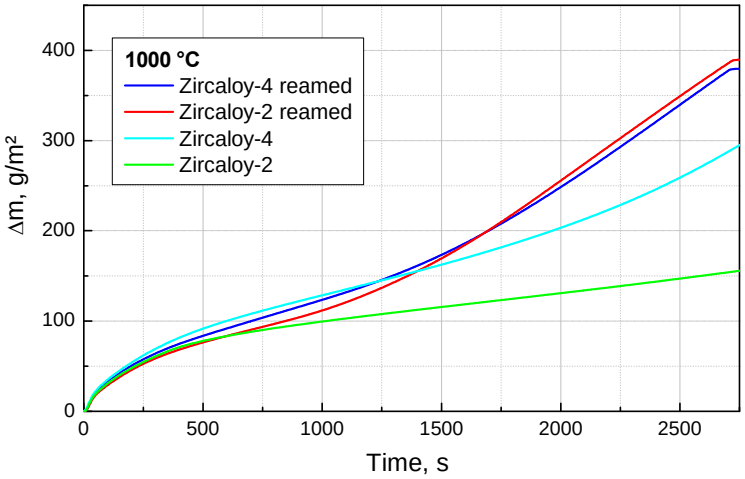

Fig. 3-5 Comparison of oxidation tests with as-received and machined samples at 1000 °C in air

Zry-4, 15 min | Zry-2, 15 min | Zry-4, 45 min | Zry-2, 45 min

Fig. 3-6 Post-test appearance of machined specimens after 15 and 45 min, respectively, oxidation in air at 1000 °C

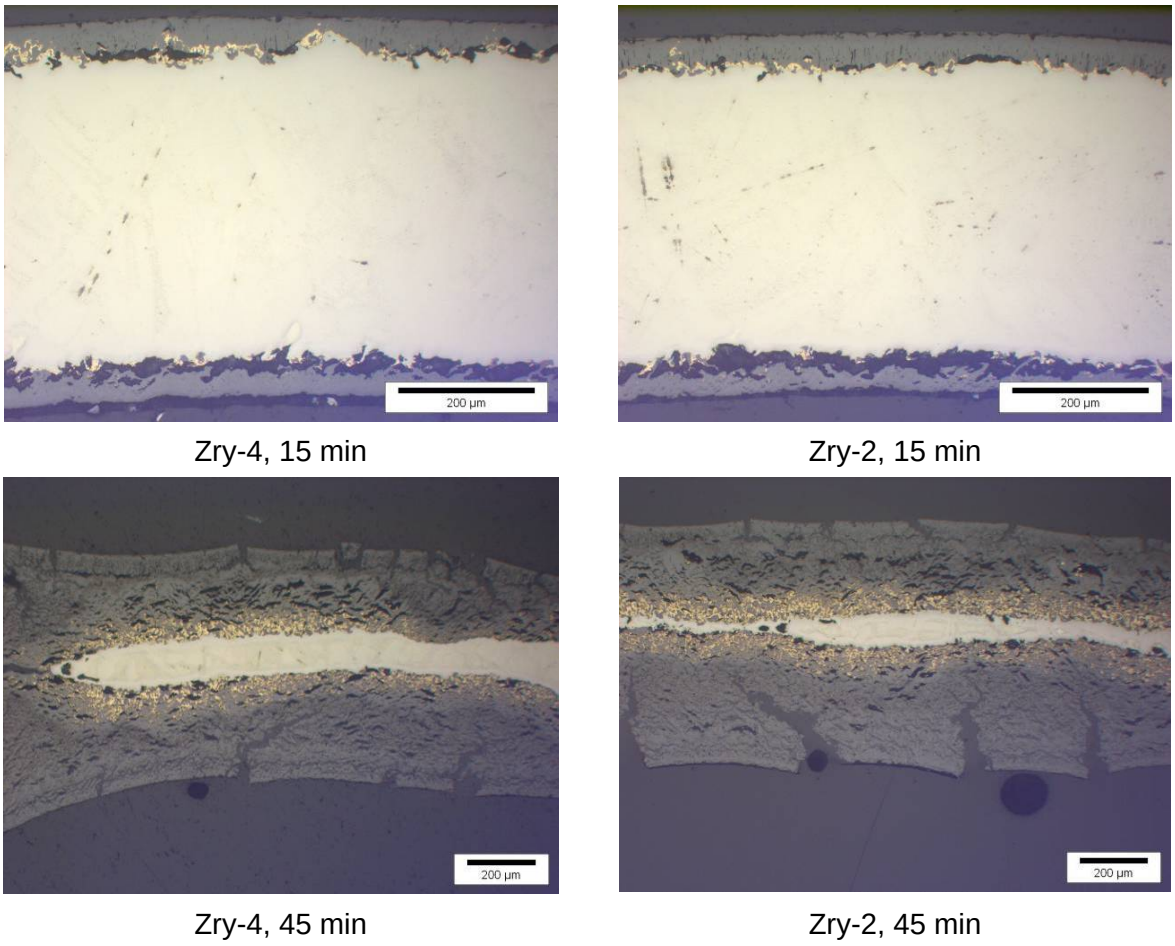

Zry-4, 15 min | Zry-2, 15 min

Zry-4, 45 min | Zry-2, 45 min

Fig. 3-7 Micrographs of machined specimens after 15 and 45 min, respectively, oxidation in air at 1000 °C

3.3 Transient oxidation experiments

The SFP experiments are transient ones; so it was reasonable to compare Zircaloy-2 and Zircaloy-4 under transient conditions. Three heating rates, namely 5, 20, and 50 K/min were chosen for this test series in the temperature range from room temperature to 1400 °C with machined samples. The comparison between the two alloys shows very similar or even identical oxidation behavior (see Fig. 3-8) and post-test appearance of the samples (see Fig. 3-9).

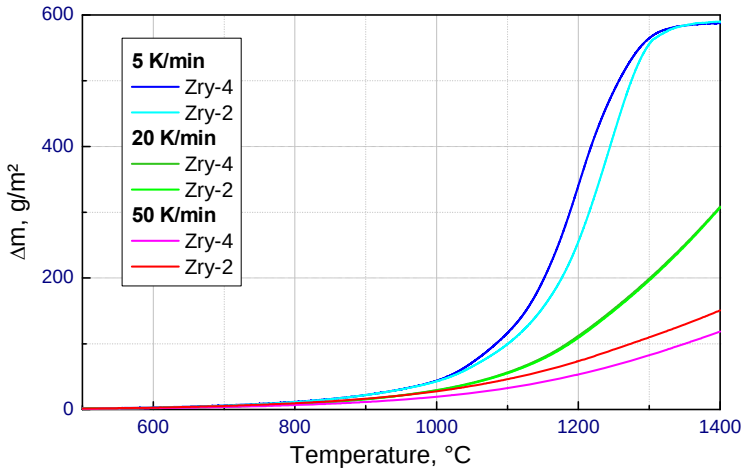

Fig. 3-8 Mass gain vs. temperature during transient oxidation of Zry-2 and Zry-4 in air

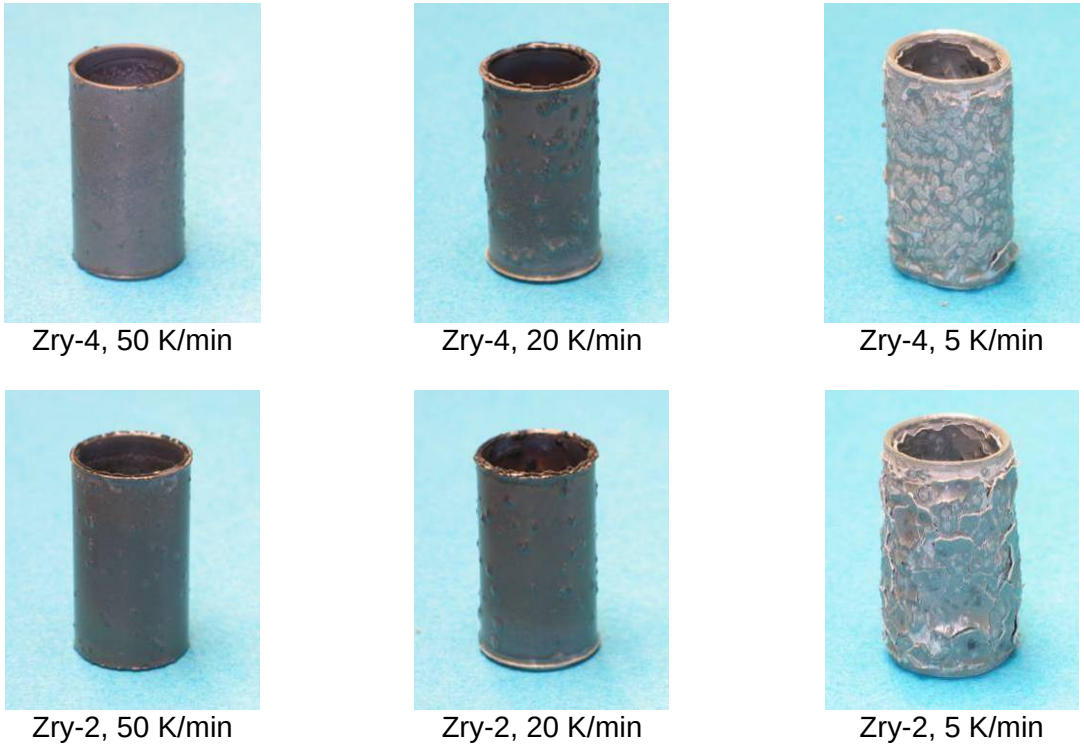

Fig. 3-9 Post-test appearance of Zry-2 and Zry-4 specimens after transient tests between RT and 1400 °C

3.4 Simulation of SFP pre-ignition and ignition tests

Even more interesting was the simulation of the SFP pre-ignition and Phase I (single bundle) ignition tests. The temperature-time characteristics were taken from MELCOR pre-test calculations [3] and [4].

The main question regarding the **pre-ignition test simulation** was to which extent the cladding will be oxidized after the two weeks lasting tests at temperatures between room

temperature and 550 °C. Test conduct and mass gain measured by TG are shown in Fig. 3-10. Only 4.4 mg mass gain due to oxidation mainly during the first phase of the test was obtained, corresponding to 3.8 g/m^2 and 2 µm oxide scale thickness, respectively. The light-blue curve in Fig. 3-10 is the as-received TG signal which is affected by drag and buoyancy; the dark-blue signal is corrected by a reference measurement without Zry specimen and smoothing procedure.

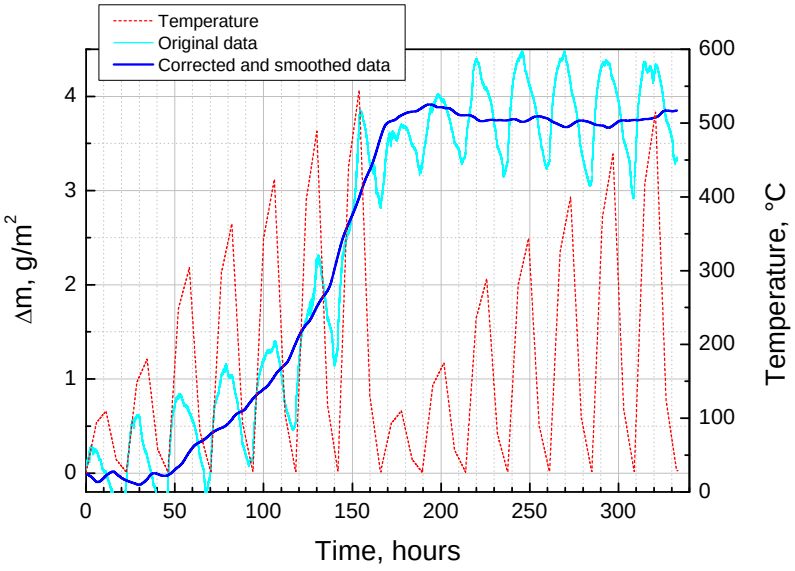

Fig. 3-10 Temperature and mass gain during pre-ignition test simulation

For the **ignition test simulation** an axially maximum temperature course according simulation of 160 days aging of the fuel element in the pool was chosen after consultation of the SNL team. Three tests were conducted up to the pre-calculated point in time of self-ignition of the bundle and up to one hour before and after this time (see Fig. 3-11). The ignition phase itself was not simulated, so the samples could be used to define the degree of oxidation just before ignition.

Figure 3-12 shows an excellent reproducibility of the three tests with an increase of the oxidation kinetics after about 8.5 hours at about 800 °C. The three tests were terminated in the region with a higher slope of the TG curve leading to strongly different mass gains at the end of the tests (40, 120, 230 g/m^2). This is also confirmed by the metallographic post-test examinations (see Fig. 3-13 and Table 3-1).

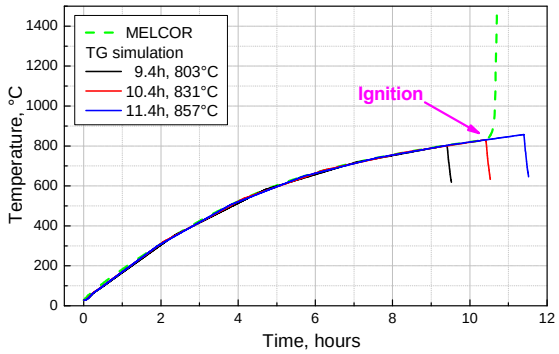

Fig. 3-11 Temperature course of simulation test of the SFP test phase I with single bundle

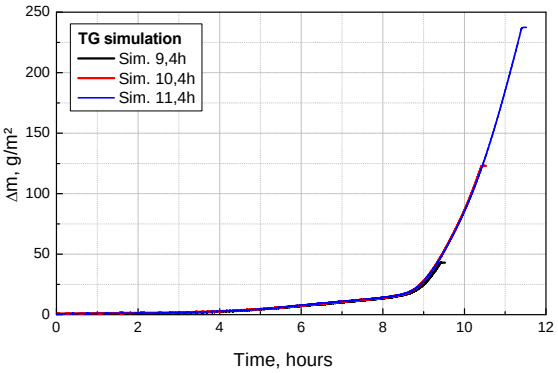

Fig. 3-12 Mass gain of SFP simulation tests with three different times till start of ignition

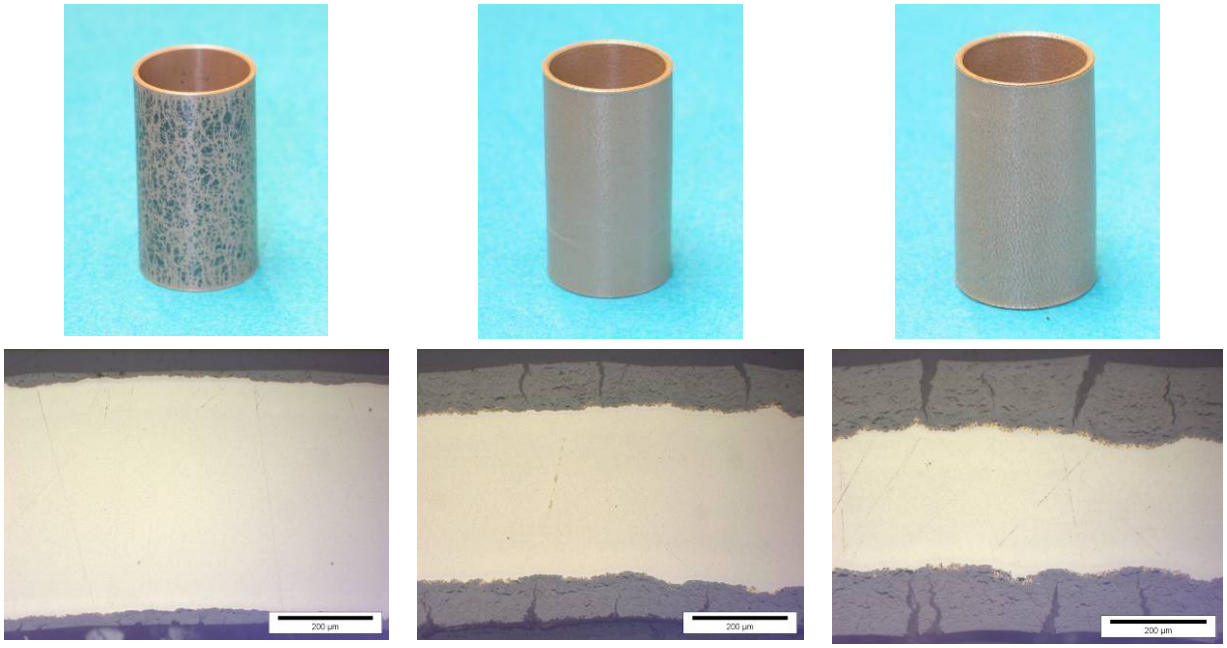

9.4 hours 10.4 hours 11.4 hours

Fig. 3-13 Post-test appearance and micrographs of Zry-2 samples after SFP Phase I simulation terminated one hour before, at the point in time, and one hour after the pre-calculated start of ignition of the test bundle

Tab. 3-1 Thicknesses of ZrO_2, α-Zr(O), and ZrN layers after SFP Phase I simulation tests

	9.4 hours	**10.4 hours**	**11.4 hours**
ZrO_2	17 µm	86µm	143 µm
α-Zr(O)	5 µm	8 µm	12 µm
ZrN	2 µm	4 µm	9 µm

The thickness of the oxide scales strongly increases from test to test. They are very porous and interspersed with radial and circumferential cracks. The α-Zr(O) layer remained relatively thin which is typical for breakaway oxidation. Zirconium nitride inclusions were found in all specimens at the phase boundary metal-oxide. More images and figures of these three tests are given in Annex E.

3.5 Mechanical tests

Mechanical experiments were carried out with non-oxidized Zircaloy-4 claddings, Zircaloy-2 claddings and two types of prototype heater rods from Zircaloy-2, respectively. The ring compression tests were performed displacement controlled, with a constant traverse velocity of 1 mm/min up to a maximum displacement of 8.5 mm and/or a maximum load of 3 kN, respectively. From every tube type, 3 rings were prepared and tested. Fig. 3-14 shows an overview of the results. One can see that the specimens from the original claddings deliver identical results, whereas the specimens from the heater rods show increasing variation of the deformation behavior with increasing loading.

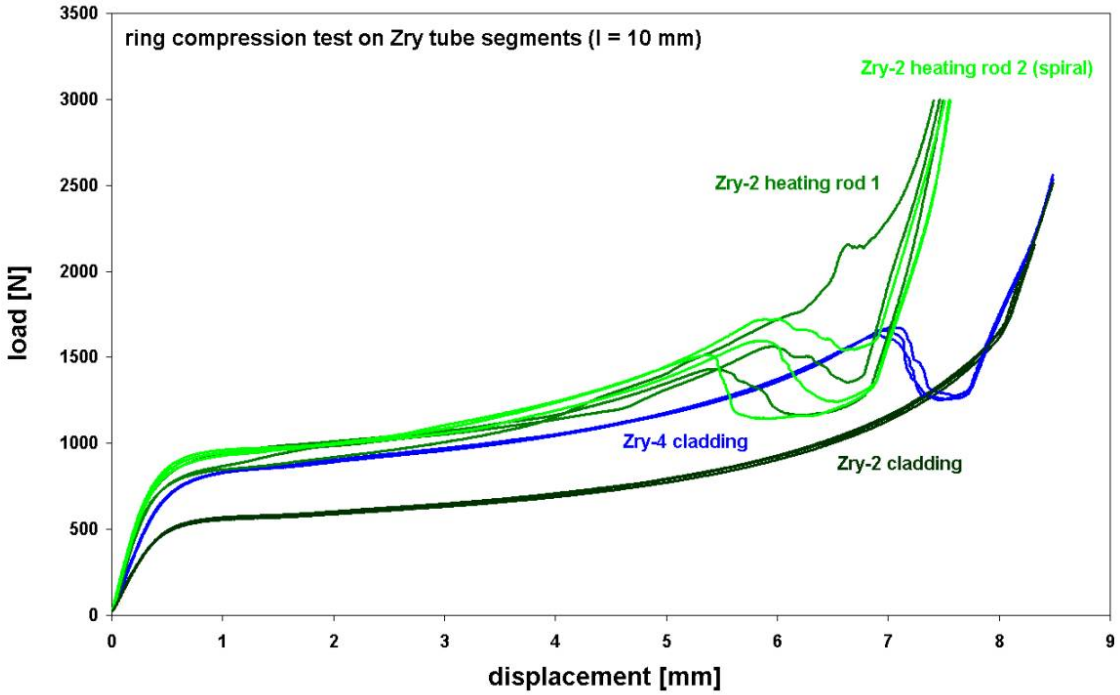

Fig. 3-14 Results of the ring compression tests

The tensile tests were also performed displacement controlled, with a traverse velocity of 2 mm/min. To determine accurate values of the Young's Modulus and the 0.2 % proof stress, respectively, a clip gauge was used within the tests. The stresses were calculated based on average values of the tubes wall thicknesses, measured at both ends of the tubes and the elongation after fracture was determined by measuring the length of a specimen before and after the test (= Δl; $\varepsilon_f = \Delta l/l$, with l = free clamping length). As one can see in Fig. 3-15, the heater rods from Zircaloy-2 clearly show higher strength values and lower elongations after fracture then the original cladding. Compared with the results of the ring compression tests, the tensile tests also deliver significant differences in terms of the deformation behavior of the two types of heating rods. In general, both, tensile tests and ring compression tests show

that in the as-delivered state Zircaloy-2 is more ductile then Zircaloy-4, whereas the strength is lower.

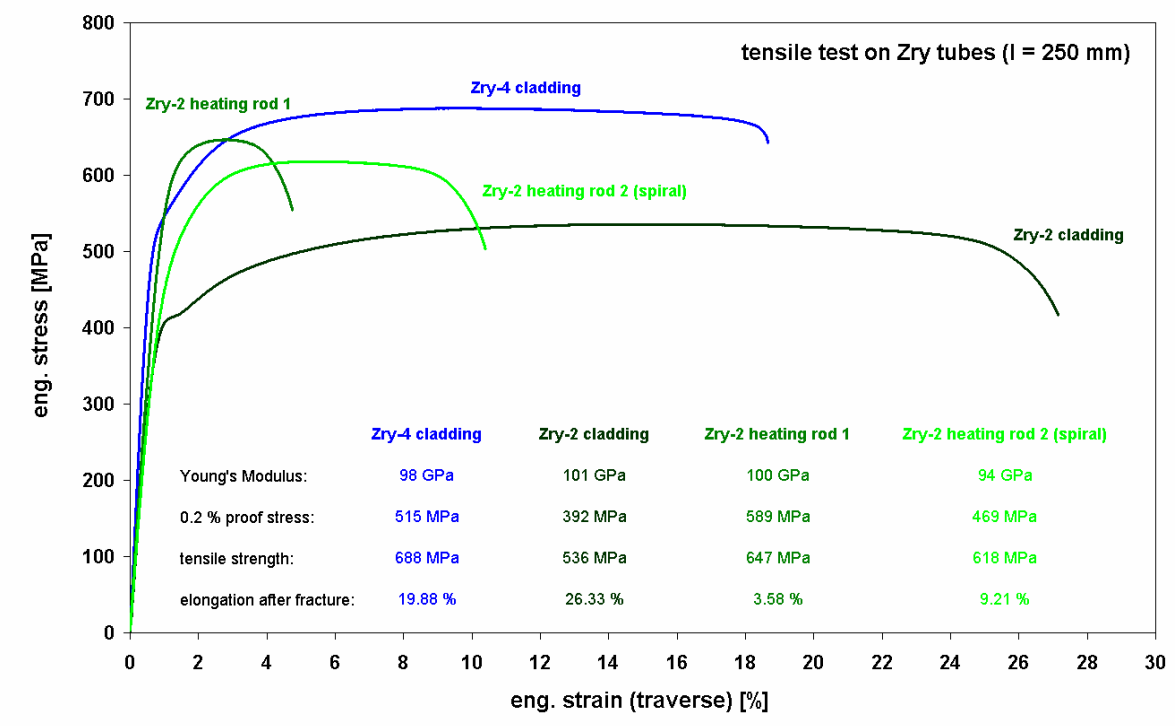

Fig. 3-15 Results of the tensile tests

4 Summary, discussion and conclusions

The oxidation and mechanical behaviour of Zircaloy-2 was studied in comparison to Zircaloy-4 in the framework of the OECD-NEA Sandia Fuel Program (SFP). Oxidation rates in air were determined in the temperature range 600-1400°C in isothermal experiments in a thermal balance. Additionally, transient tests at various heating rates were conducted as well as tests simulating the calculated scenario in a Loss of Coolant Accident (LOCA) in a spent fuel pool. The mechanical properties of the claddings were determined by ring compression and tensile tests.

The oxidation tests with as-received cladding tube segments revealed the positive effect of the inner zirconium liner on the oxidation properties of Zircaloy-2. The susceptibility to breakaway oxidation in the temperature range 600-1000 °C was strongly reduced for the as-received Zry-2 in comparison to Zry-4 and the machined claddings with removed Zr liner. This finding is rather of general interest and will not influence the SFP bundle tests with only external oxidation and insignificant interaction between the MgO filler and the inner cladding surface during the test phases before ignition.

The oxidation of the pure Zircaloy-2 (i.e. without inner Zr liner) and Zircaloy-4 alloys is very similar. The oxidation kinetics before the transition to breakaway is even identical within the range of the experimental uncertainties as can be seen in Fig. 4-1. The data and the fitting

curves of the two test series lie on the top of each other in the Arrhenius diagram and are also identical with data obtained with Zircaloy-4 obtained in 2009 [7]. It should be mentioned that the parabolic oxidation constants according to Equs. 4.1 and 4.2 have been obtained by fitting the linear part of the dm=f(sqrt(t)) curve without consideration of initial effects and the part of the curve after transition, and also neglecting the fact that especially at lower temperatures cubic rate equations better described the data. The parabolic parameters of the data obtained in this study and some literature data are summarized in Table 4-1.

$$\frac{\Delta m}{S} = k \cdot \sqrt{t} \tag{4.1}$$

$$k = k_0 \cdot \exp\left(\frac{-E_A}{RT}\right) \tag{4.2}$$

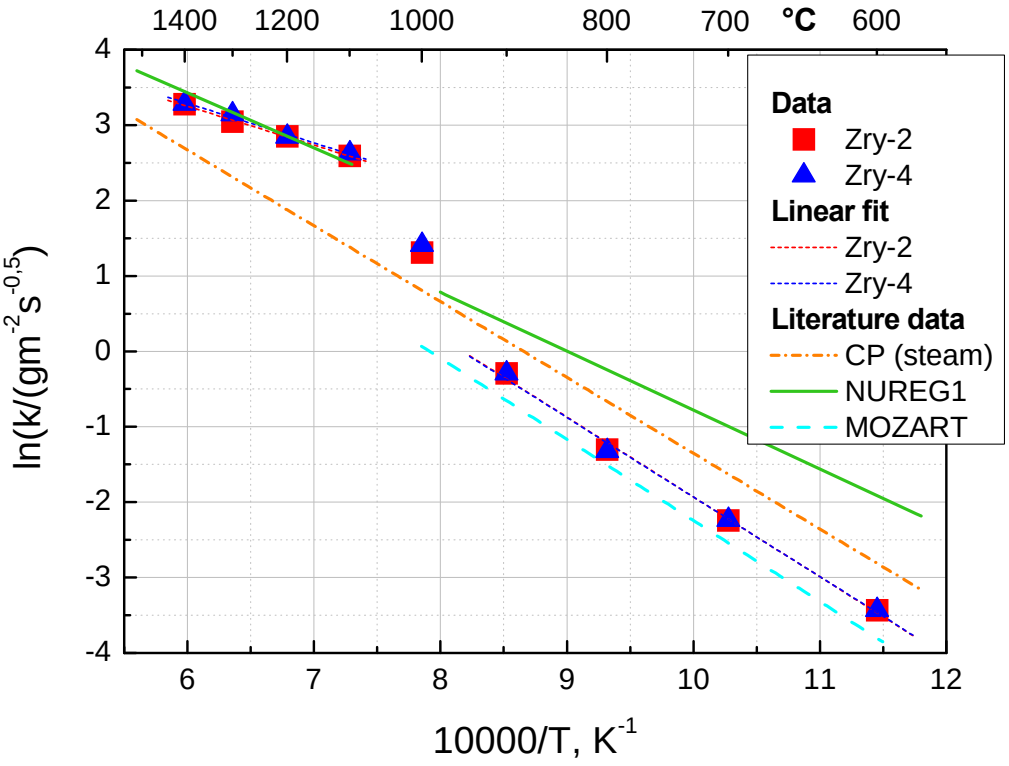

Fig. 4-1 Comparison between parabolic oxidation rates in air (before transition to faster kinetics) of Zry-2 with Zry-4 as well as with NUREG-1 [6] and MOZART [2] correlations and the Cathcart-Pawel [5] correlation for oxidation of Zry-4 in steam

Tab. 4-1 Parameters of parabolic rate constants k [$gm^{-2}s^{-0.5}$] obtained in this study and in relevant earlier work on Zry-4

Source	Temperature, K	k_0, $gm^{-2}s^{-0.5}$	E_A, J/mol
Zry-4 (this study)	873-1173	5539	87744
	1373-1673	620.3	43533
Zry-2 (this study	873-1173	5773	88072
	1373-1673	569.7	42885
Cathcart-Pawel [5] (steam)	1273-1773	6020	83600
NUREG-1 [6] (air)	<1333	1137	64978
	>1550	2490	60837
MOZART [2] (air)	873-1273	4958	89403

At higher temperatures the data of this study excellently correspond to the NUREG-1 correlation [6] which is mostly used in severe accident codes for the description of the Zry-air reaction. At lower temperatures a better correspondence is given with IRSN data recently obtained in the frame of the ISTP MOZART program [2]. For comparison, the well known and generally accepted Cathcart-Pawel correlation [5] for the oxidation of Zircaloy-4 in steam is additionally given in Fig. 4-1 and Tab. 4-1.

Transient tests, and especially the simulation of the SFP Phase 1 test scenario, have confirmed the almost identical oxidation behaviour of Zry-2 and Zry-4. The main outcome in the latter test was the sensible dependence of the degree of oxidation of the cladding tubes on the time of self-ignition of the test bundle. Here it has to be mentioned that the temperature chosen for the simulation was the maximum bundle temperature obtained by MELCOR pre-test calculations.

The two weeks lasting pre-ignition tests at temperatures between room temperature and 820 K results in an only low pre-oxidation and should have no significant effect on the main test.

In general, the tensile tests as well as the ring compression tests show that in the as-delivered Zircaloy-2 is more ductile then Zircaloy-4, whereas the strength is lower. However, especially the Zircaloy-2 heating rod 1 shows almost the same strength as the Zircaloy-4 cladding, whereas the ductility is clearly lower. Considering the results from oxidation tests, where it was observed that both alloys show comparable oxidation behavior, one has to expect a strong embrittlement of a Zircaloy-2 heating rod type 1 and thus, a strong decrease of the residual strength during the PWR SFP tests. To illustrate the impact of oxide layers on the entire mechanical behavior of claddings, Fig. 4-2 shows a comparison of an as-delivered Zircaloy-4 cladding and an oxidized Zircaloy-4 tube.

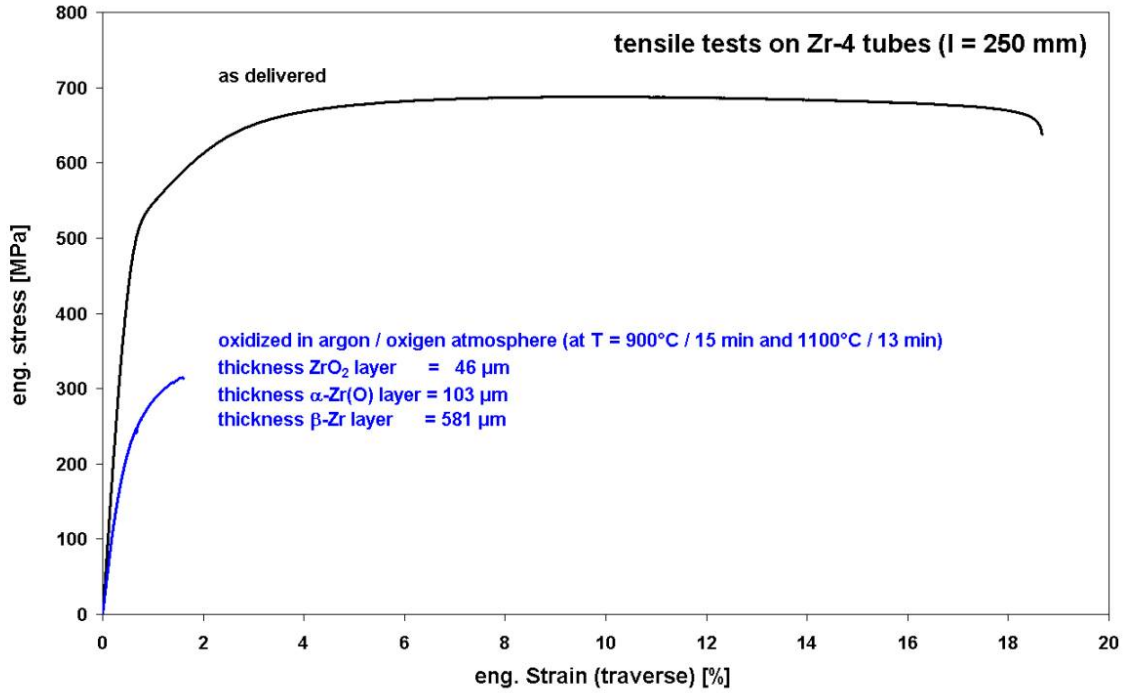

Fig. 4-2 Mechanical behavior of Zry-4 claddings; comparison: as delivered - oxidized

The final conclusions of the study are:

1. The results of the extensive experimental program revealed very similar oxidation behaviour of the two alloys Zircaloy-2 and Zircaloy-4 in the temperature range investigated. So, they are no concerns regarding the use of the BWR alloy Zircaloy-2 in the PWR SFP test series at Sandia National Laboratories from this point of view.

2. During the planned pre-ignition tests only very low pre-oxidation of the cladding and so insignificant effect on the main ignition test is expected.

3. The point in time of the ignition of the bundle strongly influences the starting conditions for the further progression of the test, especially the degree of pre-oxidation and therewith the amount of remaining metal.

4. The mechanical properties of the two alloys in the as-received state and the heater cladding are significantly different. The manufacturing process of the heater rods caused increase of strength and reduction of ductility. Further strong changes of mechanical properties are expected during course of the tests due to oxidation. This has to be taken into account for the analyses of the tests.

5 References

[1] M. Steinbrück, Prototypical experiments relating to air oxidation of Zircaloy-4 at high temperatures, J. Nucl. Mater. 392 (2009), 531-544

[2] C. Duriez, T. Dupont, B. Schmet, F. Enoch, Zircaloy-4 amd M5(R) high temperature oxidation and nitriding in air, J. Nucl. Mater. 380 (2008), 30-45

[3] E.R. Lindgren, S.G. Durbin, Characterisation of Hydraulic and Ignition Phenomena of Pressurized Water Reactor Fuel Assemblies: Phase I Test Plan, Report SAND2009-7868, Sandia National Laboratories, 2009

[4] E.R. Lindgren, private information, 2010

[5] J.V. Cathcart et al., Zirconium metal-water oxidation kinetics, IV: Reaction rate studies, Report ORNL/NUREG-17, 1977

[6] D.A. Powers et al., A Review of Technical Issues of Air Ingress During Severe Reactor Accidents, Report NUREG/CR-6218, SAND94-0731, 1994

[7] M. Steinbrück, Air oxidation of Zircaloy-4, M5® and Zirlo™ cladding alloys at high temperatures, NuMat 2010: The Nuclear Materials Conference, 4-7 October 2010, Karlsruhe, Germany

[8] http://www.wahchang.com/pages/products/data/pdf/Zr_Alloys%20for%20Nuclear%20Waste%20Dspsl.pdf

Annex A Composition of Zry-2 and Zry-4 [8]

Name UNS grade	**Zircaloy-2** **wt-%** R60802	**Zircaloy-4** **wt-%** R60804
Aluminum	0.0075	0.0075
Boron	0.00005	0.00005
Cadmium	0.00005	0.00005
Carbon	0.027	0.027
Chromium	0.05-0.15	0.07-0.13
Cobalt	0.002	0.002
Copper	0.005	0.005
Hafnium	0.01	0.01
Hydrogen	0.0025	0.0025
Iron	0.07-0.20	0.18-0.24
Iron + Chromium	--	0.28-0.37
Iron + Chromium + Nickel	0.18-0.38	--
Magnesium	0.002	0.002
Manganese	0.005	0.005
Molybdenum	0.005	0.005
Nickel	0.03-0.08	0.007
Nitrogen	0.008	0.008
Oxygen	Per P.O.	Per P.O.
Phosphorus	--	--
Silicon	0.012	0.012
Tin	1.20-1.70	1.20-1.70
Titanium	0.005	0.005
Tungsten	0.01	0.01
Uranium (total)	0.00035	0.00035

Annex B Test matrix and main results

Test ID	Alloy	Temp	Time	m_0	m_{pt}	Δm	Δm	Ar	Air	Remarks:
		°C		g	g	%	g/m²	l/h	l/h	
Isothermal tests with as-received specimens										
100409a	Zry-2	1000	30min	2.9439	3.1114	5.7	127.2	3	10	white cracks
100409b	Zry-2	1100	20min	2.8268	3.3726	19.3	414.4	3	10	axially inhomogeneous
100412a	Zry-2	1000	30min	2.9147	3.0814	5.7	126.6	3	10	white cracks
100412b	Zry-2	900	2h30min	2.944	3.0747	4.4	99.2	3	10	mushroom shaped sample
100413a	Zry-4	1000	30min	2.9539	3.1913	8.0	187.9	3	10	white cracks
100414a	Zry-4	900	2h30min	3.0061	3.3582	11.7	278.7	3	10	mushroom shaped sample
100415a	Zry-4	1100	20min	2.9433	3.5267	19.8	461.8	3	10	axially inhomogeneous
100415b	Zry-4	1200	15min	2.9602	3.5931	21.4	501.0	3	10	axially inhomogeneous
100415c	Zry-4	1300	10min	2.9185	3.5464	21.5	497.1	3	28.58	axially inhomogeneous
100415d	Zry-4	800	7h	2.9412	3.2385	10.1	235.4	3	10	brown colored sample
100416a	Zry-4	1400	10min	2.9772	3.6157	21.4	505.5	3	28.58	
100416b	Zry-2	1200	15min	2.95	3.5204	19.3	433.1	3	10	
100416c	Zry-2	600	60h	2.9042	2.9458	1.4	31.6	3	10	brown colored sample
100419a	Zry-2	1300	10min	2.9417	3.5416	20.4	455.5	3	28.58	axially inhomogeneous
100419b	Zry-2	800	7h	2.949	3.1448	6.6	148.7	3	10	axially inhomogeneous

Test ID	Alloy	Temp	Time	m_0	m_{pt}	Δm	Δm	Ar	Air	Remarks:
		°C		g	g	%	g/m²	l/h	l/h	
100420a	Zry-2(H1)	900	2h30min	2.5733	2.7685	7.6	176.5	3	10	axially inhomogeneous
100420b	Zry-4	700	17h	2.9434	3.1152	5.8	136.0	3	10	brown colored sample
100421a	Zry-2(H1)	1000	30min	2.5297	2.6607	5.2	118.4	3	10	white cracks
100421b	Zry-2(H1)	1100	20min	2.5383	3.0086	18.5	425.2	3	10	axially inhomogeneous
100421c	Zry-2	700	17h	2.9354	3.0332	3.3	74.3	3	10	brown colored sample
100422a	Zry-2	1400	10min	3.0222	3.6725	21.5	493.8	3	28.58	
100422b	Zry-2	1000	1h20min	3.0143	3.3375	10.7	245.4	3	10	white cracks
100423a	Zry-4	1000	1h20min	3.0224	3.8572	27.6	660.9	3	10	white cracks
100423b	Zry(H2)	1100	20min	2.6869	3.204	19.2	467.5	3	10	axially inhomogeneous
100423c	Zry-4	600	60h	3.0157	3.0846	2.3	54.5	3	10	brown colored sample
100427a	Zry-2(H2)	1000	30min	2.6841	2.8272	5.3	129.4	3	10	white cracks
100427b	Zry-2(H2)	900	2h30min	2.6901	2.835	5.4	131.0	3	10	mushroom shaped sample
Isothermal tests with reamed specimens										
100427c	Zry-2R	700	17h	2.2848	2.4875	8.9	151.1	3	10	brown colored sample
100428a	Zry-2R	1000	45min	2.2821	2.8326	24.1	410.4	3	10	white cracks
100428b	Zry-4R	700	17h	2.1759	2.3499	8.0	134.7	3	10	brown colored sample
100429a	Zry-4R	1000	45min	2.1797	2.6992	23.8	402.1	3	10	white cracks
100429b	Zry-2R	1300	10min	2.2819	2.778	21.7	369.8	3	10	axially inhomogeneous

Test ID	Alloy	Temp	Time	m_0	m_{pt}	Δm	Δm	Ar	Air	Remarks:
		°C		g	g	%	g/m²	l/h	l/h	
100430a	Zry-4R	1300	10min	2.1813	2.6758	22.7	382.8	3	10	axially inhomogeneous
100430b	Zry-4R	1000	45min	2.1763	2.6869	23.5	395.2	3	10	white cracks
100430c	Zry-2R	600	60h	2.282	2.3577	3.3	56.4	3	10	brown colored sample
100503b	Zry-2R	800	7h	2.2862	2.638	15.4	262.2	3	10	mushroom shaped sample
100504a	Zry-2R	900	1h20min	2.286	2.463	7.7	131.9	3	10	mushroom shaped sample
100505a	Zry-2R	1400	10min	2.2902	2.7531	20.2	345.1	3	10	
100505b	Zry-4R	900	1h20min	2.175	2.2975	5.6	94.8	3	10	mushroom shaped sample
100505c	Zry-4R	800	7h	2.1659	2.4901	14.9	250.9	3	10	brown colored sample
100506a	Zry-2R	1300	7.5min	2.2819	2.8719	25.9	439.8	3	28.58	axially inhomogeneous
100506b	Zry-4R	1300	7.5min	2.1793	2.7552	26.4	445.8	3	28.58	axially inhomogeneous
100506c	Zry-2R	1400	7min	2.2796	2.8179	23.6	401.3	3	28.58	
100507a	Zry-4R	1400	7min	2.1649	2.6852	24.0	402.7	3	28.58	
100507b	Zry-2R	1200	15min	2.2786	2.8433	24.8	420.9	3	10	
100507c	Zry-4R	1200	15min	2.1677	2.7068	24.9	417.3	3	10	
100510a	Zry-2R	1100	15min	2.2803	2.7671	21.3	362.9	3	10	axially inhomogeneous
100510b	Zry-4R	1100	15min	2.1722	2.661	22.5	378.4	3	10	axially inhomogeneous
Transient tests										
100511a	Zry-2R	20K/min		2.2849	2.7063	18.4	314.1	3	10	surface bumps

Test ID	Alloy	Temp	Time	m_0	m_{pt}	Δm	Δm	Ar	Air	Remarks:
		°C		g	g	%	g/m²	l/h	l/h	
100511b	Zry-4R	20K/min		2.1602	2.5662	18.8	314.3	3	10	surface bumps
100512a	Zry-2R	5K/min		2.2726	3.0637	34.8	589.7	3	10	oxide spalling
100525a	Zry-4R	5K/min		2.177	2.9361	34.9	587.6	3	10	oxide spalling
100526a	Zry-2R	50K/min		2.2801	2.5335	11.1	188.9	3	10	
100526b	Zry-4R	50K/min		2.1811	2.4276	11.3	190.8	3	10	
Simulation SFP ignition test										
100607a	Zry-2R		10.4h	2.2794	2.4473	7.4	125.2	3	10	brown colored
100609a	Zry-2R		11.4h	2.2845	2.6128	14.4	244.7	3	10	brown, swollen
100610a	Zry-2R		9.4h	2.2841	2.3419	2.5	43.1	3	10	brown cracks
Repetition tests										
100527a	Zry-2	900	2h30min	2.9617	3.1258	5.5	124.6	3	10	
100528a	Zry-2R	1000	15min	2.2822	2.4435	7.1	120.2	3	10	
100528b	Zry-4R	600	60h	2.1803	2.2516	3.3	55.2	3	10	
100531a	Zry-4R	1000	15min	2.1738	2.3326	7.3	122.9	3	10	
100601a	Zry-2	800	7h	3.0302	3.207	5.8	134.2	3	10	
100615a	Zry-4	900	2h30min	3.0328	3.469	14.4	345.3	3	10	
100615b	Zry-2	900	2h30min	3.0276	3.2181	6.3	144.6	3	10	
100616a	Zry-4	800	7h	2.9981	3.3054	10.2	243.3	3	10	

Annex C Post-test appearance of Zry-2 and Zry-4 samples after isothermal oxidation tests

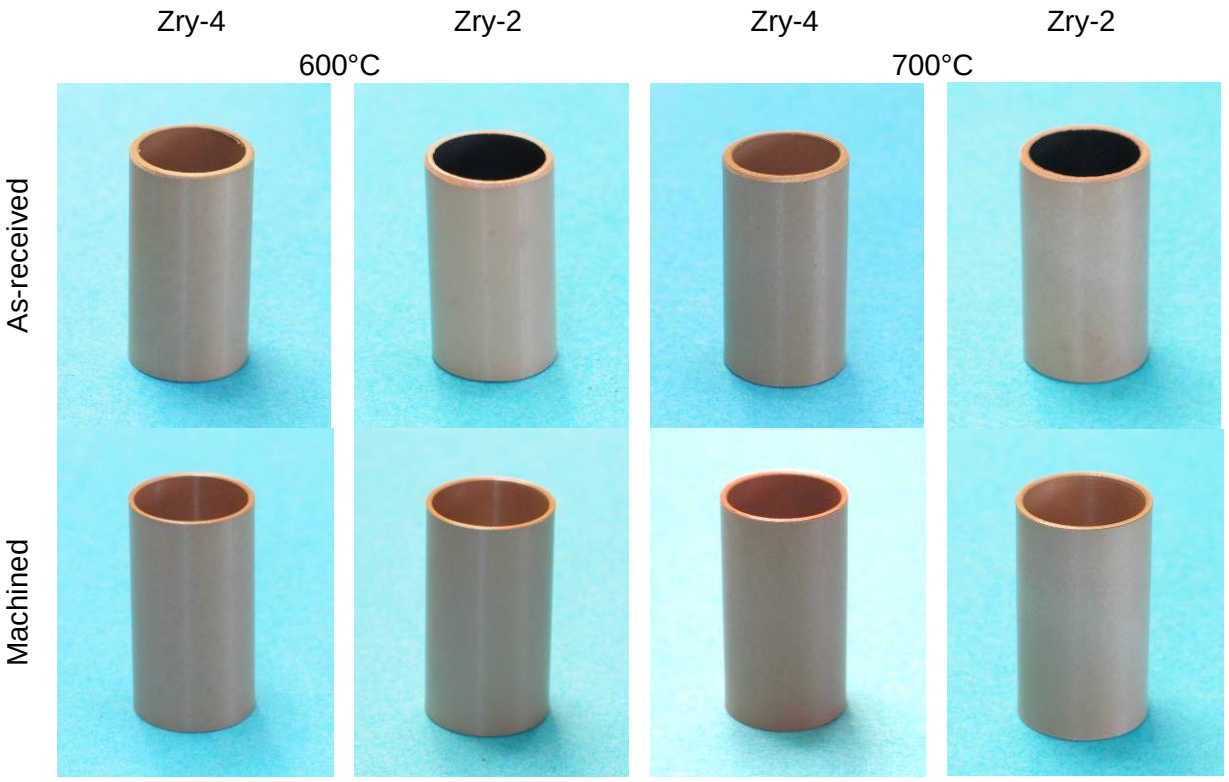

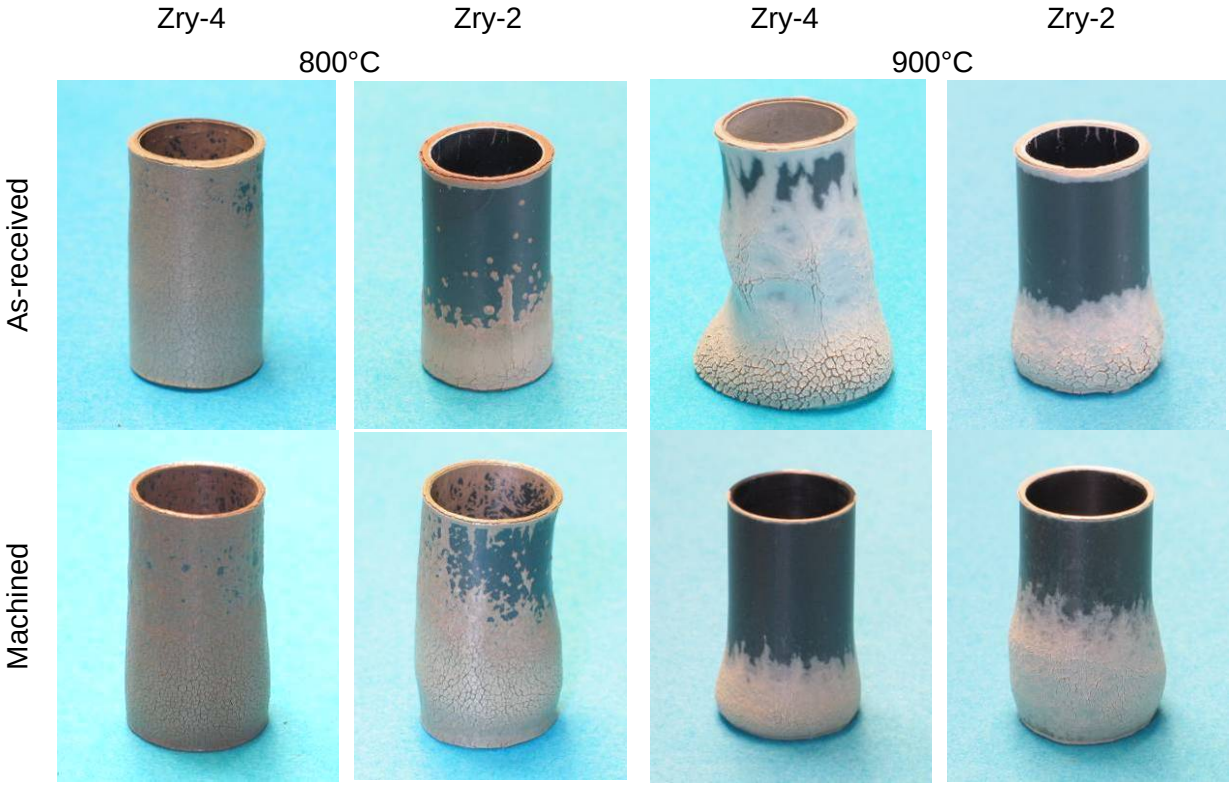

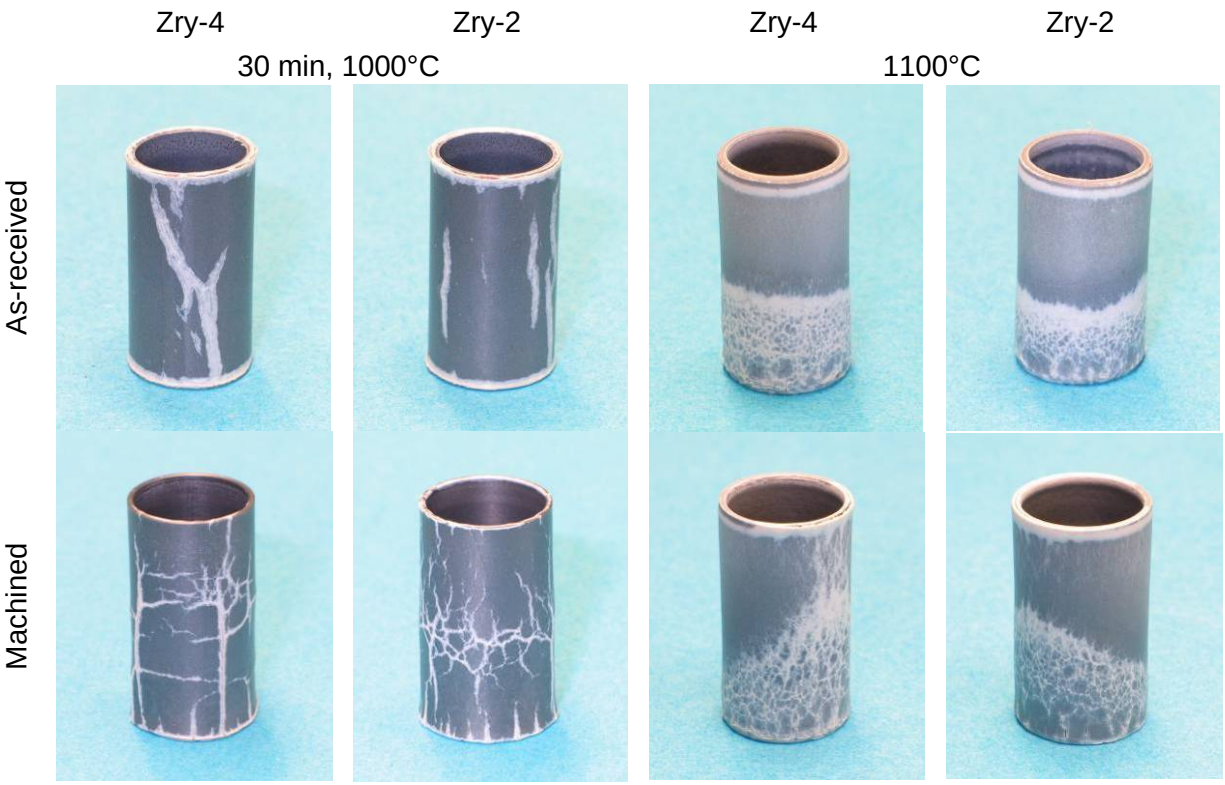
Zry-4
Zry-2
Zry-4
Zry-2
30 min, 1000°C
1100°C
As-received
Machined

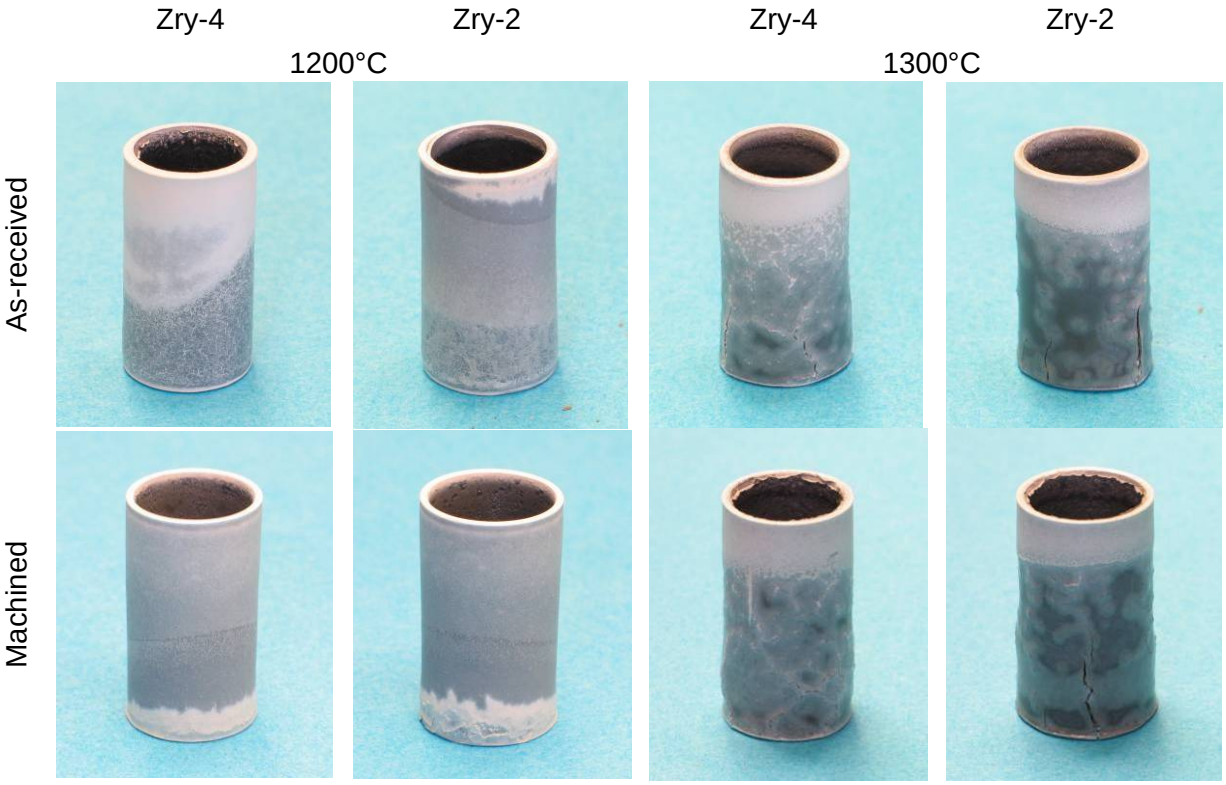
Zry-4
Zry-2
Zry-4
Zry-2
1200°C
1300°C
As-received
Machined

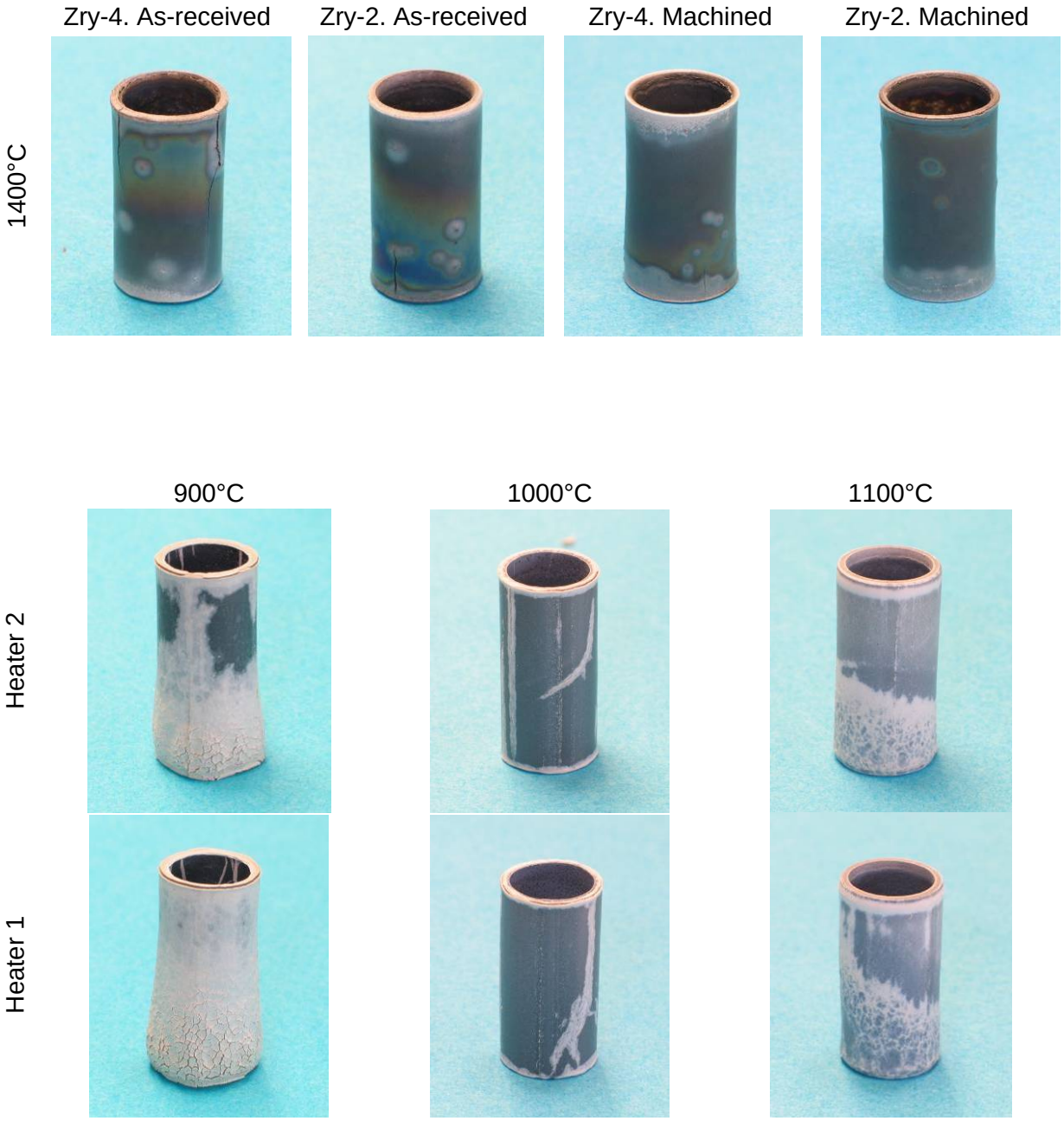
Zry-4. As-received
Zry-2. As-received
Zry-4. Machined
Zry-2. Machined
1400°C
900°C
1000°C
1100°C
Heater 2
Heater 1

Annex D Micro images of Zry-2 and Zry-4 cross sections after isothermal oxidation tests

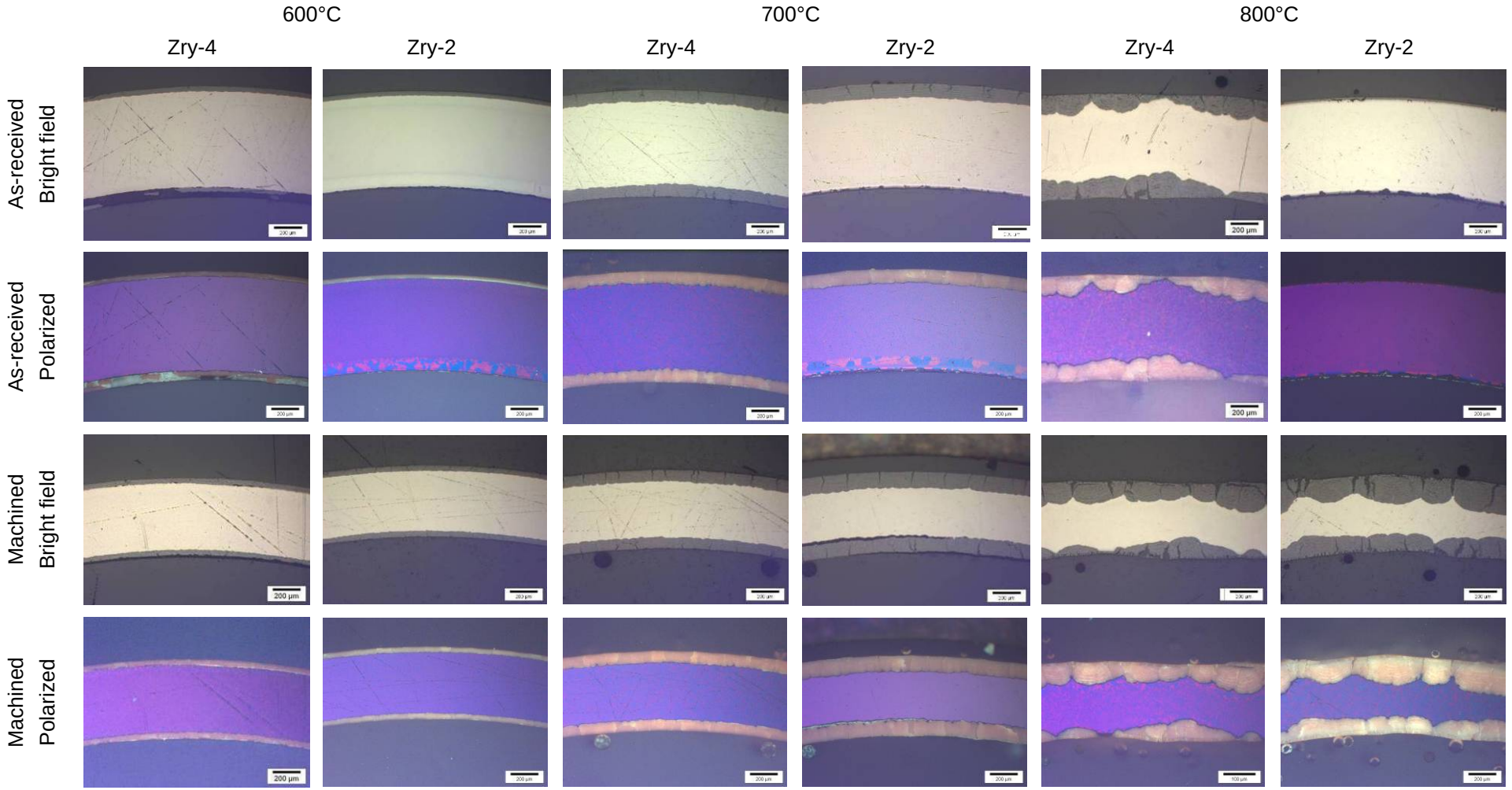

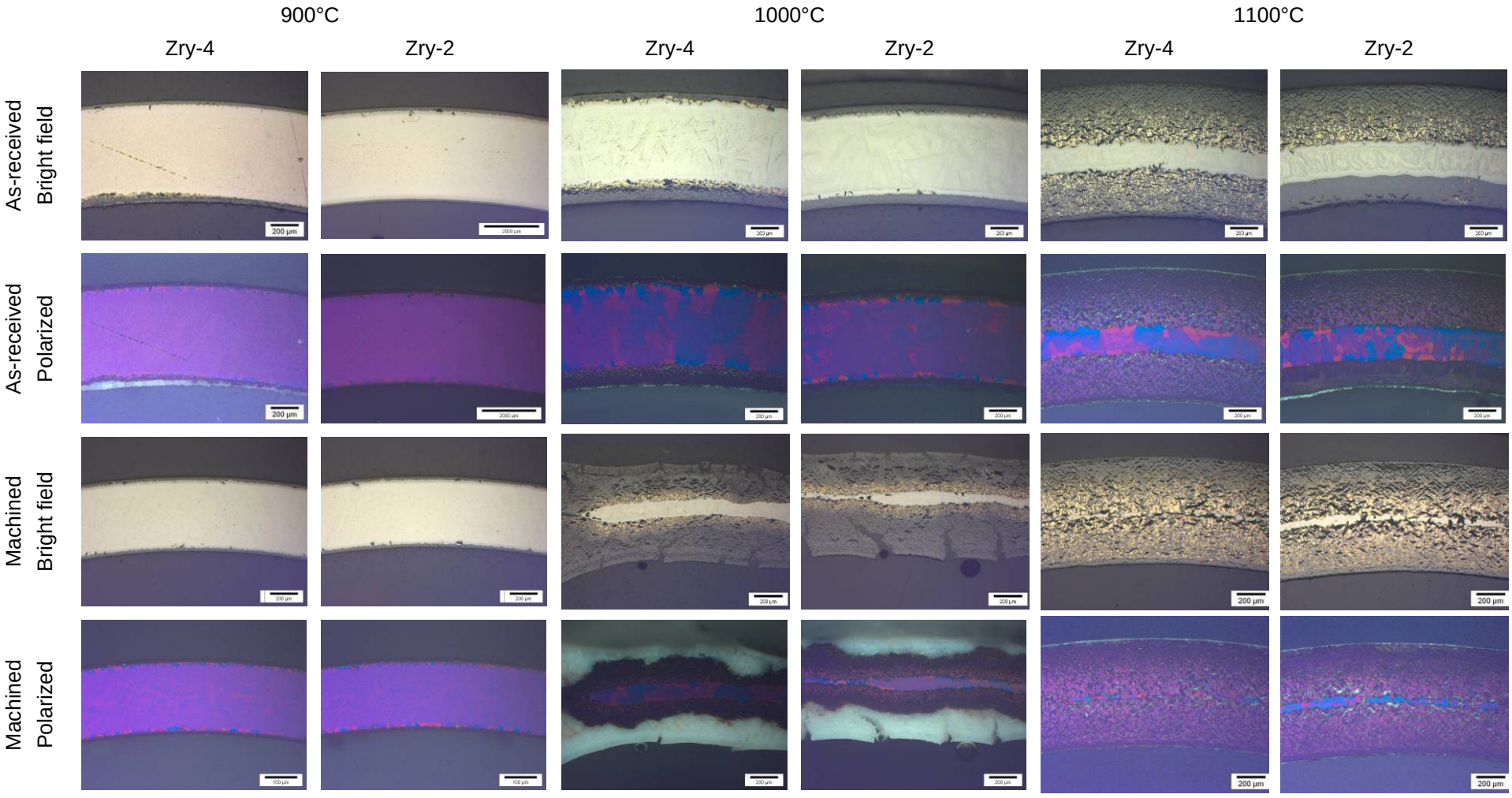
900°C
1000°C
1100°C
Zry-4
Zry-2
Zry-4
Zry-2
Zry-4
Zry-2
As-received Bright field
As-received Polarized
Machined Bright field
Machined Polarized
200 µm

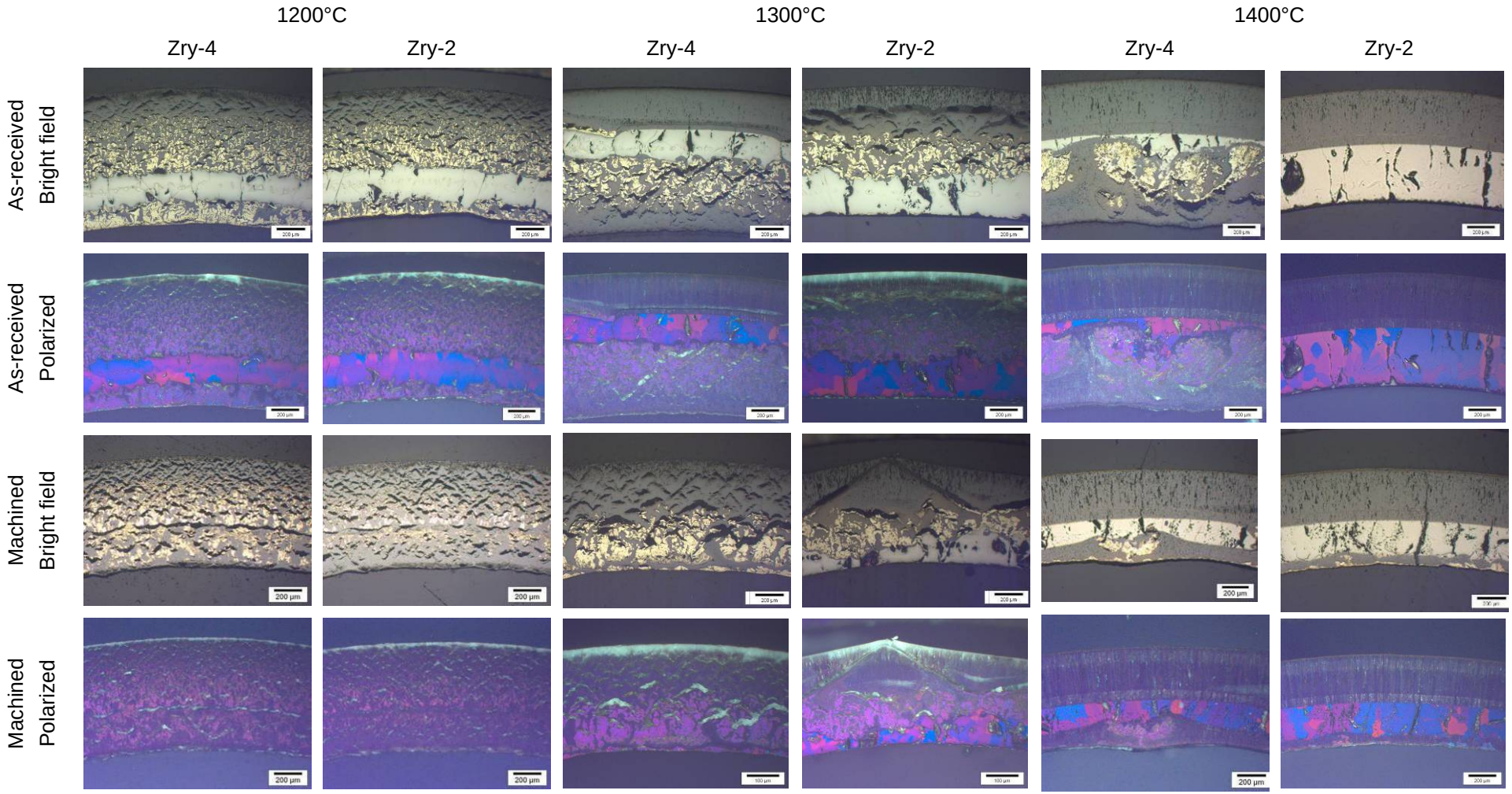
1200°C
1300°C
1400°C
Zry-4
Zry-2
Zry-4
Zry-2
Zry-4
Zry-2
As-received Bright field
As-received Polarized
Machined Bright field
Machined Polarized

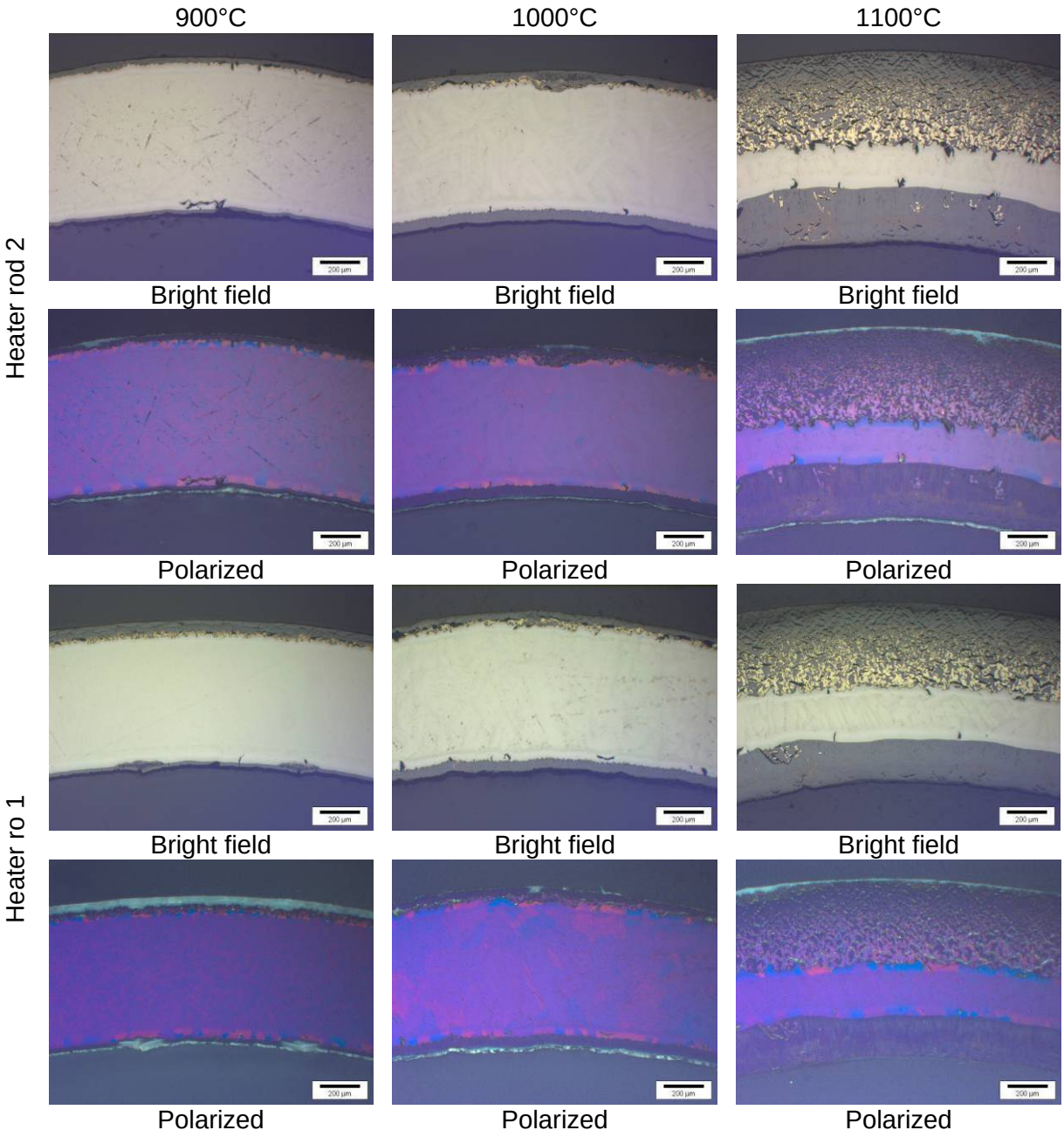
900°C
1000°C
1100°C
Heater rod 2
Bright field
Bright field
Bright field
Polarized
Polarized
Polarized
Heater ro 1
Bright field
Bright field
Bright field
Polarized
Polarized
Polarized

Annex E Post-test images of the SFP Phase I simulation tests with measurements

9.4 hours

10.4 hours

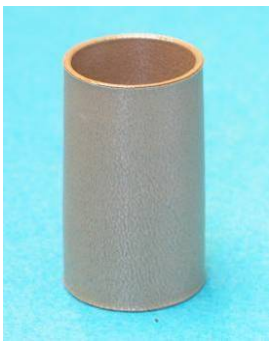

11.4 hours

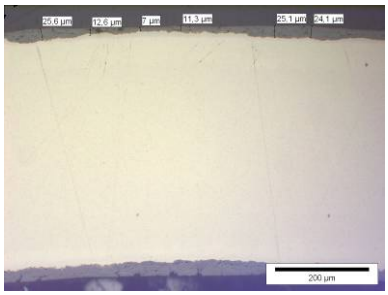

Bright field. ZrO_2

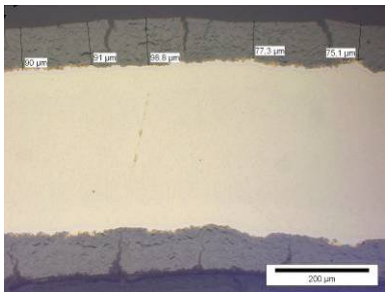

Bright field. ZrO_2

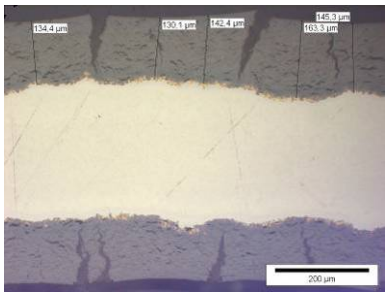

Bright field. ZrO_2

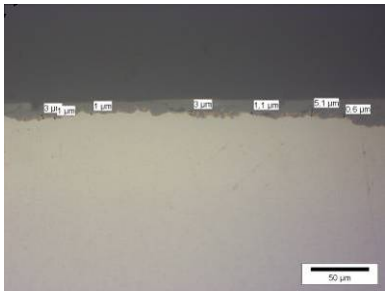

Bright field. ZrN

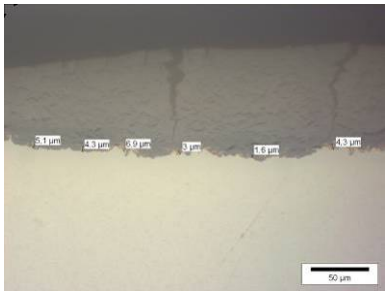

Bright field. ZrN

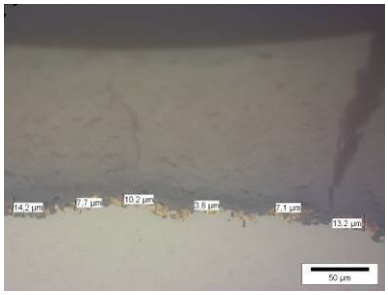

Bright field. ZrN

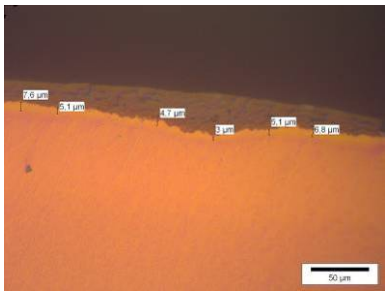

Polarized. α-Zr(O)

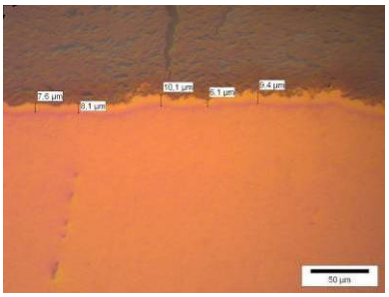

Polarized. α-Zr(O)

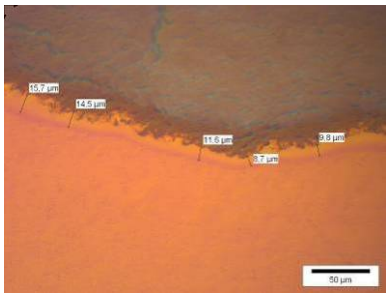

Polarized. α-Zr(O)